

INFORMATION TO USERS

This manuscript has been reproduced from the microfilm master. UMI films the text directly from the original or copy submitted. Thus, some thesis and dissertation copies are in typewriter face, while others may be from any type of computer printer.

The quality of this reproduction is dependent upon the quality of the copy submitted. Broken or indistinct print, colored or poor quality illustrations and photographs, print bleedthrough, substandard margins, and improper alignment can adversely affect reproduction.

In the unlikely event that the author did not send UMI a complete manuscript and there are missing pages, these will be noted. Also, if unauthorized copyright material had to be removed, a note will indicate the deletion.

Oversize materials (e.g., maps, drawings, charts) are reproduced by sectioning the original, beginning at the upper left-hand corner and continuing from left to right in equal sections with small overlaps.

ProQuest Information and Learning
300 North Zeeb Road, Ann Arbor, MI 48106-1346 USA
800-521-0600

UMI[®]

University of Alberta

A High Load MEMS Sensor for Use in Scoliosis Correction Surgery

by

David Craig Benfield



A thesis submitted to the Faculty of Graduate Studies and Research in partial fulfillment of
the

requirements for the degree of *Master of Science*

Department of *Mechanical Engineering*

Edmonton, Alberta
Fall 2005



Library and
Archives Canada

Bibliothèque et
Archives Canada

0-494-09123-1

Published Heritage
Branch

Direction du
Patrimoine de l'édition

395 Wellington Street
Ottawa ON K1A 0N4
Canada

395, rue Wellington
Ottawa ON K1A 0N4
Canada

Your file *Votre référence*

ISBN:

Our file *Notre référence*

ISBN:

NOTICE:

The author has granted a non-exclusive license allowing Library and Archives Canada to reproduce, publish, archive, preserve, conserve, communicate to the public by telecommunication or on the Internet, loan, distribute and sell theses worldwide, for commercial or non-commercial purposes, in microform, paper, electronic and/or any other formats.

The author retains copyright ownership and moral rights in this thesis. Neither the thesis nor substantial extracts from it may be printed or otherwise reproduced without the author's permission.

AVIS:

L'auteur a accordé une licence non exclusive permettant à la Bibliothèque et Archives Canada de reproduire, publier, archiver, sauvegarder, conserver, transmettre au public par télécommunication ou par l'Internet, prêter, distribuer et vendre des thèses partout dans le monde, à des fins commerciales ou autres, sur support microforme, papier, électronique et/ou autres formats.

L'auteur conserve la propriété du droit d'auteur et des droits moraux qui protègent cette thèse. Ni la thèse ni des extraits substantiels de celle-ci ne doivent être imprimés ou autrement reproduits sans son autorisation.

In compliance with the Canadian Privacy Act some supporting forms may have been removed from this thesis.

Conformément à la loi canadienne sur la protection de la vie privée, quelques formulaires secondaires ont été enlevés de cette thèse.

While these forms may be included in the document page count, their removal does not represent any loss of content from the thesis.

Bien que ces formulaires aient inclus dans la pagination, il n'y aura aucun contenu manquant.


Canada

Dedicated to my parents.

Abstract

Scoliosis surgery is a complicated procedure during which steel rods are fixed to vertebrae of the spine in order to correct abnormal curvature. This procedure places three dimensional forces and moments on the spine, which are of interest as they can be a factor in operative success rates and may be useful for pre-surgical planning, educational training and increasing knowledge of the spine's mechanical properties. A design is presented to measure these three-dimensional forces and moments, modifying the hooks and screws used to affix the rods to the spine. Specifically, a set of piezoresistive MEMS force sensors will be positioned between the hook or screw and the rod. Information collected by these sensors will then be sent with an onboard wireless transmitter to a storage and real-time display unit. Viability testing and characterization of this sensor design is presented in two main categories: finite element analysis and prototype testing.

Acknowledgements

This project is truly the work of many, and I am delighted to be a part of it. I became acquainted with this project while working as a COOP student at the Glenrose Rehabilitation Hospital, which was certainly one of the best jobs I've ever had. My experiences there account for much of my motivation to begin graduate studies, and all of my interest in biomedical engineering. I would like to thank Dr. Moreau and Dr. Mahood, for always keeping the practical goals of this project in sight and for making the observation of surgery as comfortable as possible. I would also like to thank Kajsa Duke for her work on this project, without which I wouldn't have had a place to begin. Finally, I'd like to thank Jim Raso, Doug Hill and everyone else that I've worked with at the Glenrose for their ongoing support, organization and frequent proofreading.

Regarding my work at the U of A, I would like to acknowledge my supervisors, Dr. Walied Moussa and Dr. Edmond Lou. These two have provided guidance and a great working environment for completing this project. I have never stopped being impressed with how they can share so much of their knowledge and experience without making things stressful. I also must mention the team at the Nanofab, primarily Shane and Aruna, who were hugely helpful with my prototype trials. The final tip of my hat goes to the MEMS/Multiphysics Design Group that I've been a part of for over two years now. The relaxed atmosphere and good people make doing research casual and productive.

Thanks also go out to my friends and family, who made sure I got out of the lab to have some fun once in a while.

Table of Contents

Chapter 1 – Problem Description	1
1.1 – Background	1
<i>1.1.1 – Description of Scoliosis</i>	1
<i>1.1.2 – Surgical Treatment</i>	1
<i>1.1.3 – Previous Work Measuring Loads</i>	2
1.2 – Motivation	3
1.3 – Objectives	4
1.4 – Proposed Solution	5
<i>1.4.1 – Description of Sensor System</i>	5
<i>1.4.2 – Operation of Sensor</i>	6
Chapter 2 – Current Technology and Background Information	14
2.1 – Literature Review of Applicable Technology	14
2.2 – Finite Element Analysis Theory	15
<i>2.2.1 – Introduction to FEA</i>	15
<i>2.2.2 – Specification of FEA Parameters</i>	16
2.3 – Contact Analysis Theory	17
<i>2.3.1 – Contact Theory</i>	17
<i>2.3.2 – Contact Simulation</i>	18
2.4 – Description of Square Diaphragm Deformation	19
<i>2.4.1 – Diaphragm Deflection Theory</i>	19
<i>2.4.2 – Diaphragm Deflection Simulation</i>	21
2.5 – Description of the Piezoresistive Effect	21
<i>2.5.1 – Piezoresistive Theory for Four-Terminal Gauges</i>	21
<i>2.5.2 – Simulation of the Four Terminal Gauge</i>	23
Chapter 3 – Proof of Proposed Solution	30
3.1 – Detailed Device Description	30
<i>3.1.1 – Layout Overview</i>	30

3.1.2 – <i>Strip Placement</i>	30
3.1.3 – <i>Pad Placement</i>	31
3.1.4 – <i>Membrane Details and Piezoresistive Sensor Placement</i>	31
3.2 – Contact Loading Applied in the Normal Loading Scenario	33
3.2.1 – <i>Device Symmetry and Finite Element Modeling</i>	33
3.2.2 – <i>Calculated Contact Loads</i>	34
3.3 – Numerical Evaluation of Output Voltages	34
3.3.1 – <i>Piezoresistive Sub-Model</i>	34
3.3.2 – <i>Calculated Voltage Outputs</i>	35
3.3.3 – <i>Sensor Pad Calibration Equations</i>	35
Chapter 4 – Evaluation of Device Output Sets	44
4.1 – Loading Scenario Descriptions	44
4.1.1 – <i>Definition of Coordinate Systems</i>	44
4.1.2 – <i>Description of Applied Loads</i>	45
4.2 – Resolving Loads from Input Voltages	46
4.3 – Prototype Manufacturing	47
4.3.1 – <i>Motivation</i>	47
4.3.2 – <i>Prototype Sensor Description</i>	48
4.4 – Prototype Performance Evaluation	50
4.4.1 – <i>Comparison Methodology</i>	50
4.4.2 – <i>Finite Element Characterization</i>	50
4.4.3 – <i>Experimental Characterization</i>	51
4.4.4 – <i>Prototype Characterization Results</i>	52
Chapter 5 – Conclusions	63
5.1 – Achieved Objectives	63
5.2 – Continued Development	64
5.3 – Concluding Remarks	65
Bibliography	67

List of Tables

Table 2.1. 'Exact' equations for deflections and bending moments in a uniformly loaded square plate with fixed edges.	20
Table 2.2. Westergaard equations for deflections and bending moments in a uniformly loaded square plate with fixed edges.	21
Table 3.1. Sensitivities of a test pad under shear and normal loading.	36
Table 4.1. Expected signal patterns during hook load application.	45
Table 4.2. Calculated values for sensor output in a hypothetical M_2 load application scenario.	47

List of Figures

Figure 1.1a. Pre-operative x-ray of a scoliotic spine.	8
Figure 1.1b. Post-operative x-ray of a scoliotic spine.	9
Figure 1.2. The instrumented rod rotator system.	10
Figure 1.3. A scoliosis hook instrumented with strain gauges.	10
Figure 1.4. Schematic of rod-hook/rod-screw interface.	11
Figure 1.5. Sensor instrumentation attached to the hook or screw head.	12
Figure 1.6. Cut-away view of the silicon substrate strip with piezoresistive areas shaded.	12
Figure 1.7. Load application on the rod and the equivalent distribution on the sensing strips.	13
Figure 1.8. Visualization of a load distribution (R_1 or R_2) applied to a sensor strip.	13
Figure 2.1. Schematic of elastic cylinder contact for the Hertz and Smith-Liu equations.	25
Figure 2.2. A comparison of numerical and analytical stress distributions in a sensor strip.	25
Figure 2.3. Error calculation for numerical contact width as a function of mesh size.	26
Figure 2.4. Coordinate system used for derivation of membrane equations.	26
Figure 2.5. Comparison of theoretical and numerical membrane deflection for a 1mm square membrane under a 100kPa pressure load.	27
Figure 2.6. Schematic of the four-terminal gauge.	27
Figure 2.7. Sensitivity of the four-terminal gauge as it is rotated.	28
Figure 2.8. Zero voltage as a function of mesh size.	29
Figure 3.1. Cutaway view of the sensor strip in a hook notch.	38
Figure 3.2. Membrane sensor numerical test model.	39
Figure 3.3. Rotated membrane sensor numerical test model.	39
Figure 3.4. Hook/screw model used for normal loading contact analyses with planes of symmetry shown.	40
Figure 3.5. Numerical results for membrane deformation (μm units).	41
Figure 3.6. Numerical results for contact pressure on the rod (MPa units).	42

Figure 3.7. Half strip model used for piezoresistive analysis.	43
Figure 3.8. Simulated sensor outputs for the normal loading scenario.	43
Figure 4.1. Coordinate system for each hook or screw head. Letters indicate relative locations of sensor pads on the device.	55
Figure 4.2. Coordinate systems for each pad.	56
Figure 4.3. Schematic of the manufactured device.	57
Figure 4.4. Electrical connectivity of the manufactured device.	57
Figure 4.5. Piezoresistive sensor manufacturing scheme.	58
Figure 4.6. Data sets from sensor testing and simulation.	59
Figure 4.7. Sensitivity variation as ideal membrane thickness is adjusted.	59
Figure 4.8. Sensitivity variation as the force application site is moved away from diaphragm center.	60
Figure 4.9. Schematic of the sensor characterizing apparatus.	60
Figure 4.10. Photo of the sensor characterizing apparatus.	61
Figure 4.11. Cross-sectional profile of experimental sensor 1.	62
Figure 4.12. Cross-sectional profile of experimental sensor 2.	62

List of Symbols

$1,2,3$	Hook or screw coordinate system
$1,N,T$	Pad coordinate system
A	Sensor designation
a	Membrane edge length
B	Sensor designation
b	Half width of contact area
c	Stiffness tensor
C	Series term constants, sensor designation
Δ	Contact constant
D	Flexural rigidity, sensor designation
d	Rod diameter
E	Young's modulus, Electrical field
F	Force
ΣF_{app}	Sum of forces applied to the rod
f	Frictional coefficient
j	Electric current
k	Constant term
L	Hall effect sensor width
l	Contact length
M	Moment, Pad Sensitivity
ΣM_{app}	Sum of moments applied to the rod
$p(x,y)$	Membrane loading function
Q	Rotational tensor
q	Distributed load
R	Reaction loads on the sensing strips
r	Arbitrary tensor
ρ	Resistivity
π	Piezoresistivity
S	Pad load

σ	Stress
ν	Poisson's ratio
V	Voltage
W	Hall-effect sensor width
w	Membrane deflection perpendicular to the membrane

Chapter 1 – Problem Description

Scoliosis is a condition in which a patient suffers from an abnormal spinal curvature that may be corrected surgically. In the corrective procedure the spine is straightened by fixing a metal rod to the back using specialized hooks and screws. It is proposed that the three dimensional loads that are applied be measured using a wireless piezoresistive sensor system. These forces and moments are important factors in ensuring patient safety and quality of correction during surgery, and may also be useful for pre-surgical planning, educational training and increasing knowledge of the spine's mechanical properties.

1.1 – Background

1.1.1 – Description of Scoliosis

Scoliosis is characterized by abnormal curvature of the spine and axial rotation of vertebra. In 2-3% of the population, this condition is serious enough to require treatment, which consists of observation for further progression, bracing or surgery [1]. Surgery is recommended for severe cases, when the curvature angle is greater than 50° and progressing, which accounts for approximately 10% of those who require treatment [2]. Without treatment, severe curvature may cause severe physical pain, disfigurement and cardiorespiratory problems. Scoliosis can present with trunk distortion, deformity of the rib cage, asymmetrical elevation of the shoulders and hips, and prominence of a scapula [3]. In the majority of cases, scoliosis develops during adolescence with no known cause. This is referred to as adolescent idiopathic scoliosis, or AIS. Figures 1.1a and 1.1b show radiographs of a scoliotic spine before and after surgery.

1.1.2 – Surgical Treatment

Surgical correction of scoliosis is performed to prevent further progression of the spinal curvature and to reduce spinal deformity. This surgery is a complicated mechanical process utilizing a specialized spinal instrumentation system. Although some evolution of these instrumentation systems has occurred since Harrington introduced the first widely used system in the 1960's [4], the typical surgical correction involves inserting

special hooks and screws into selected vertebrae of the spine. Surgeons then secure a metal rod into notches in the heads of the hooks and screws, applying forces and moments to the spine to achieve the desired correction.

The spinal instrumentation system that is currently used for most cases at the University of Alberta Hospital is the Cotrel Doubouset (CD) system (Sofamor Danek) [5]. This system offers advantages over the Harrington rod system, as it allows scoliosis to be addressed as a three-dimensional deformity and decreases the risk of complication due to mechanical failure. The CD system consists of a pre-bent rod (or rods) placed on the spine. The rods are fixed in place by several laminar hooks or pedicle screws, located at several levels of the spine. Loads are distributed along the spine by the CD system as the surgeon performs the correction. Little work has been reported quantifying these loads; the skill and experience of the surgeon are the key factors to the success of the surgery.

1.1.3 – Previous Work Measuring Loads

There has been little documented work quantifying the loads applied and distributed along the spine during corrective surgery. Most of the work that has been done was performed many years ago [6, 7], measuring only the distortion forces applied during the Harrington rod procedure. In a study published in 2000, Rohlmann et al. [8] used telemetric instrumentation to study the loading on internal spinal fixation devices, but did not report on how loads applied by the surgeon correlate to the loads distributed along the spine. Work performed by the Scoliosis Research Group at the Glenrose Rehabilitation Hospital [9-12] has included studies of the loads applied to the spine by the surgeon during the *derotation maneuver* [11, 12] and also techniques to measure the loads from the surgeon transferred by the hooks and screws to the spine [9, 10]. Currently, further development of the instrumented hooks and screws is necessary so that three-dimensional spinal loading during surgery can be obtained.

An instrumented rod rotator system (Figure 1.2) was used in a study by Lou et al. [12] to measure forces and moments applied during the *derotation maneuver*. This device was calibrated in the laboratory and used on seven patients. The maximum loads measured during these seven surgeries ranged from 20 to 60N with moments from 4000

to 11000N-mm. Duke's system [9] measures loads applied to the spine using hooks and screws instrumented with strain gauges. Figure 1.3 shows an instrumented hook. Duke's system has significant disadvantages, the most important of which being that it is only able to detect moments about one axis and forces in a single direction, meaning that the three dimensional force and moment load that is being applied is not fully captured. Also, the strain gauges used as the load detection scheme are prone to signal drift when exposed to the humidity and contamination found in the operating room. In the orientations measured by the instrumented hooks and screws, several clinical trials found that forces reached 120N and moments reached 800N-mm. This is a significant difference from the loads measured by the instrumented rod rotator during the *derotation maneuver*. In the context of the design of a hook or screw sensor able to measure forces and moments in three dimensions, the load ranges obtained from both the rod rotator and Duke systems should be considered.

1.2 – Motivation

Ensuring that the load magnitudes are within specified tolerances is the primary reason to measure the loads applied during scoliosis correction surgery. The application of excessive forces and moments can cause bone failure at the hook or screw insertion site, and may also contribute to the development of pseudoarthroses and fatigue failure of the instrumentation. Applying insufficient loads during surgery may yield a sub-optimal correction. Additionally, evenly distributing the load over several vertebrae maintains a higher net correction load while keeping the load on each vertebra at safe levels.

Specific complications related to improper load application while using CD instrumentation have been reported in literature [5, 13, 14]. In a study of 250 patients, Cotrel [5] reported six patients suffered dislodgement of the upper hooks while two patients encountered transverse process fractures. In a study of 38 patients, Van Ooy et al. [13] reported two cases of complete implant loosening requiring surgical revision. Four had shifting at the upper level, one had dislocation of the convex lower hook and one suffered from erosion at several hook sites. In a retrospective study of 52 patients, Guidera et al. [14] reported 17 complications including hook pull out, pseudoarthrosis and rod failure. Hook pull out and instrumentation dislodgement may damage the spine

causing pain and reduced correction. Hook push in is another problem that an inappropriate load application may cause, which can increase the possibility of spinal cord damage [15]. Been [16] has reported immediate neurological complications in two patients immediately after insertion of lumbar hooks.

Increasing knowledge of the mechanical behavior of the spine is a secondary motivation for load measurement during scoliosis surgery. Statistical information of the forces and moments applied will be collected, creating quantitative ranges and averages of loads that surgeons will be able to use as reference points during surgery. Combining this statistical information with quantitative feedback information displayed in real-time during surgery will serve as surgical tool, which will be useful for both optimizing the correction and as an educational device.

With a larger sample of vertebral load and displacement data, it will be possible to implement a computer model for pre-surgical planning. This computer model could be used to guide placement of the hooks and screws, and also to predict the load levels that will provide an optimal correction while minimizing the risk involved with overloading the spine. A better presurgical planning model allows better prediction of surgical outcomes which will additionally improve operative success rates for patients.

1.3 – Objectives

The goal of this research is to instrument the Cotrel Doubouset system to measure the loads applied and distributed along the spine during surgery. Ultimately, this will include the design, simulation, manufacture and characterization of a wireless sensor capable of measuring forces and moments in three dimensions. Knowledge of the loads applied will provide a more comprehensive, quantitative understanding of the surgical procedures, which has the potential to improve operative success rates. This system should be able to display feedback information in real-time during surgery, as well as to store information for use in presurgical planning and statistical modeling. The scope of this thesis, however, is limited to the design, simulation and preliminary manufacturing of the load detection components.

The previous work performed measuring loads allows design constraints for an instrumented hook or screw able to measure forces and moments in three-dimensions to

be developed. The range of forces and moments measured with Duke's system [9] have been found to be in a non-maximum direction. The moment loads were also found to be significantly lower than those measured by the instrumented rod rotator system [12]. To account for these discrepancies, as well as to provide a factor of safety, the sensor system will be designed to handle loads of up to 1000N and 4000N-mm. Experience gained in previous studies also shows that background electronic noise is much higher in the operating room environment. To work successfully, all components of the sensor system must be able to compensate for this background noise. The sensor system must also be physically robust to survive the abuses of sterilization and surgery. Previous systems using strain gauges were very prone to wire breakage and contamination. The instrumentation has a better chance of providing usable output if it is well sealed, without any extended features that might be broken off or cavity features that may become contaminated.

1.4 – Proposed Solution

1.4.1 – Description of Sensor System

A custom design using a piezoresistive sensing scheme was adapted to meet the load constraints as described in the preceding section. In order to interfere as little as possible with the surgical protocols while still being able to measure forces and moments in three dimensions, it was determined that the best location for measuring loads would be at the rod-screw or rod-hook interfaces (a schematic of an interface with the relevant dimensions is shown in Figure 1.4). Other locations on or within the hook and screw bodies for the loads to be measured were also considered. These locations were rejected due to a lack of sensitivity or the requirement that the hooks and screws be modified or re-machined, which would be complicated and expensive. Keeping in mind that the goal of this research is to develop a wireless load sensing system to measure the forces and moments applied to the spine in real time during surgery, the following system design has evolved.

By using two sensing strips in combination within the notch of the hook or screw, the detection of forces and moments in three dimensions is possible. This detection is made possible by combining localized load values measured at several positions on each

strip (this is described in greater detail in chapters 3 and 4). Figure 1.5 depicts the design scheme with major components labeled. Sensing strips with several sensor pads on each are positioned opposite each other in the notch of the hook or screw head. These two sensing strips contact the rod at 30° angles and will be preloaded as the break-off bolt locks the rod in place. Stresses on the strips create voltage outputs that are transferred to a wireless (ZigBee) transceiver system mounted externally on the screw head. Power for the sensor (3.0V DC) is provided by a battery or other power source mounted opposite the wireless transceiver. The components are fixed in place on the screw/hook heads with epoxy, and sealed with a biocompatible adhesive coating. A laptop with a wireless receiver is used to receive the wireless signals and analyze the sensor outputs. Three-dimensional forces and moments concurrent with those applied by the surgeons are displayed and stored in real time during the correction phase of the surgery. After the correction is completed the instrumented hooks and screws are removed and replaced with non-instrumented hardware. Since the majority of this research will focus on the load detection components, the remainder of this work will be about the sensor strips.

Each sensor strip is sized to fit within the hook or screw notch. Specifically, this size is 8.3mm x 1.5mm x 0.5mm. The sensor strips are cut out of a (100), n-type silicon substrate with specific areas doped with p-type piezoresistive material, as shown in Figure 1.6. Local stress outputs are generated at two locations per strip on a structure called a “pad”. Each pad consists of four sensors on a 150µm thick diaphragm. Each sensor is a four-terminal piezoresistive gauge that produces a unique output voltage depending on the local stress distribution on the section of the pad where it is located. Since each sensor has a different sensitivity to different load directions, the direction and magnitude of the loads on each pad can be determined by the combination of output voltages from the four sensors.

1.4.2 – Operation of Sensor

During use, the surgeon will place the rod into the hook or screw notch and secure it with a break-off bolt. This action puts a preload on the sensing strips and allows forces and moments applied to the rod to be transmitted into the sensing strips as reaction loads. This transmission is illustrated in Figure 1.7 where ΣF_{app} represents the sum of the forces

applied to the rod, ΣM_{app} represents the sum of the moments applied to the rod and R_1 and R_2 represent the reaction loads distributed onto the sensing strips. Because of the complex loading on the rod, R_1 and R_2 will not be simple reaction force distributions. Each will vary along the length of the strip as shown in Figure 1.8. This variation allows unique signal outputs to be produced at each of the four pads depending upon the loads applied during surgery. Analysis of the operation of the sensor consists of determining R_1 and R_2 from a load applied to the rod by solving a contact problem, then determining the deflection of the membrane on each pad, and finally calculating the voltage outputs that each piezoresistive sensor on each pad will produce. The complexity of an analysis of the operation of this sensor makes simulation with finite element analysis (FEA) a desirable solution.

Although a prototype hook/screw sensor has not been tested yet, this project will show that the piezoresistive sensor design presented meets constraints and produces outputs usable for multi-axis load detection in a scoliosis surgery application. Finite element analysis and verification with analytical equations will be used to solve the governing equations of this simulation. Simulated outputs will then be converted into calibration equations, which will then be used to test the ability of the system to resolve three dimensional forces and moments. This project has the potential to improve surgical protocols and operative success rates, and may also lead to further integration of MEMS within biomedical engineering.

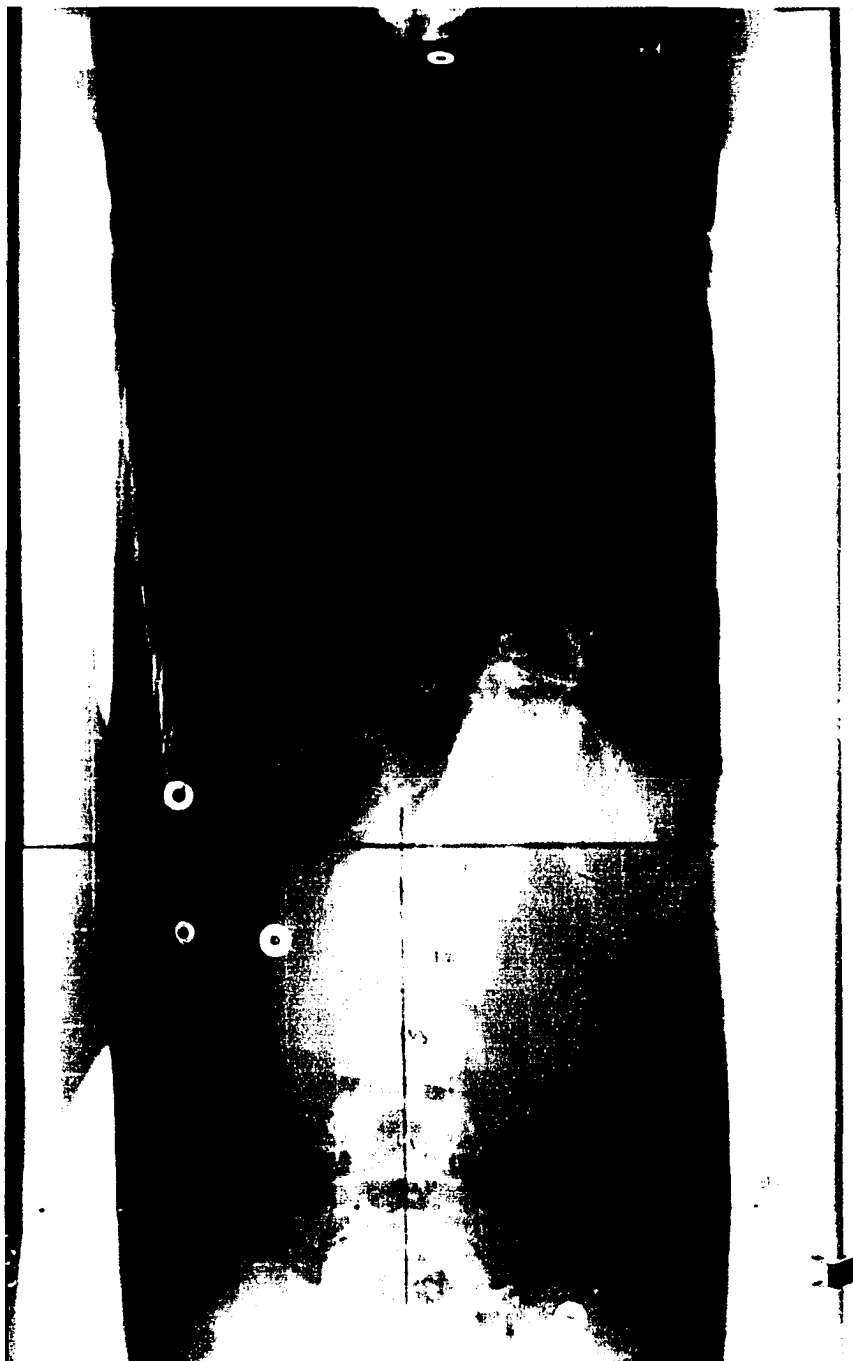


Figure 1.1a. Pre-operative x-ray of a scoliotic spine. (Photo used with permission of the Glenrose Rehabilitation Hospital.)

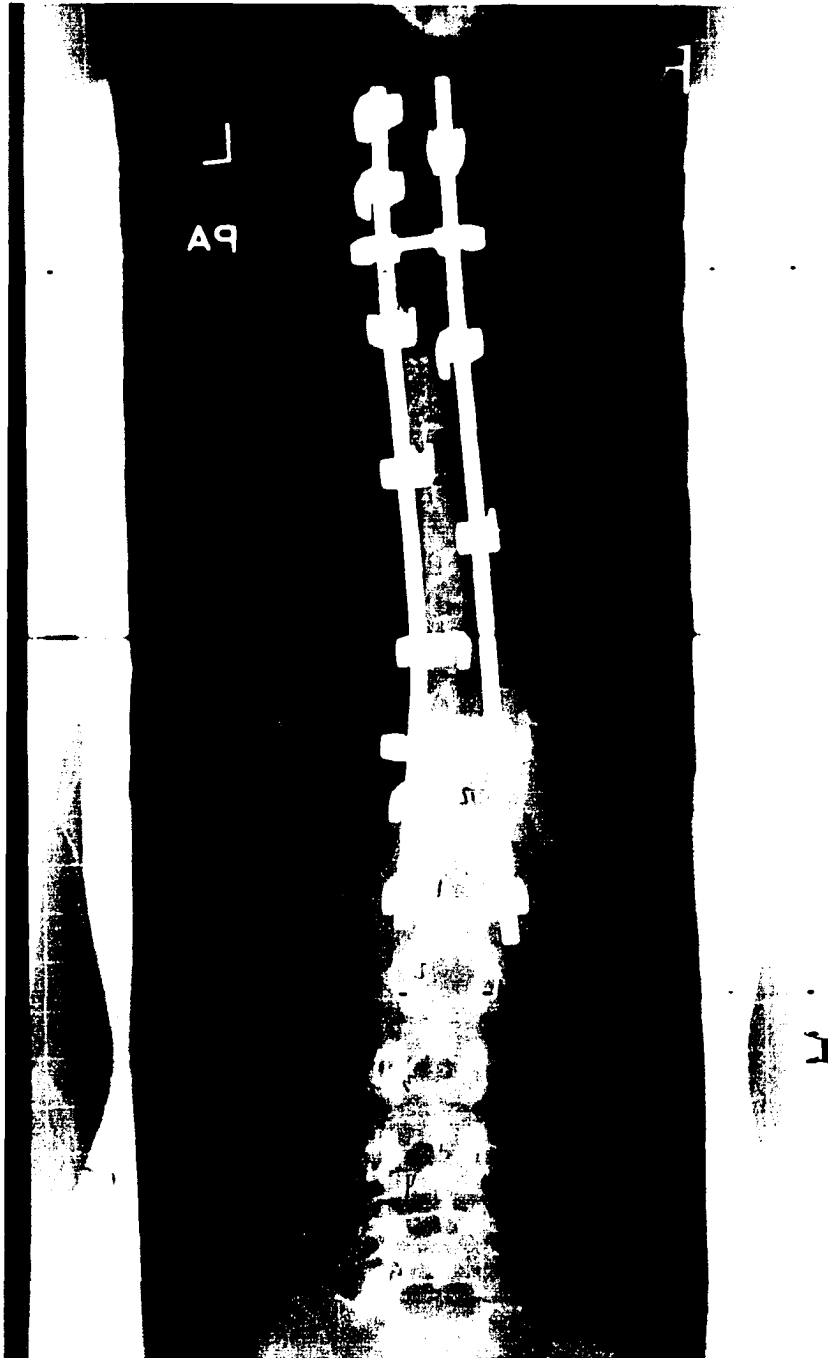


Figure 1.1b. Post-operative x-ray of a scoliotic spine. (Photo used with Permission of the Glenrose Rehabilitation Hospital.)

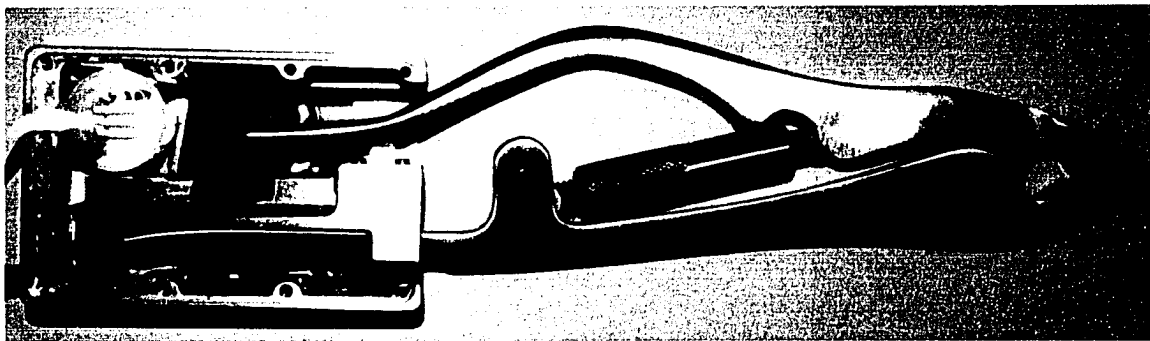


Figure 1.2. The instrumented rod rotator system. (Photo from [12]. Used with the permission of the authors.)

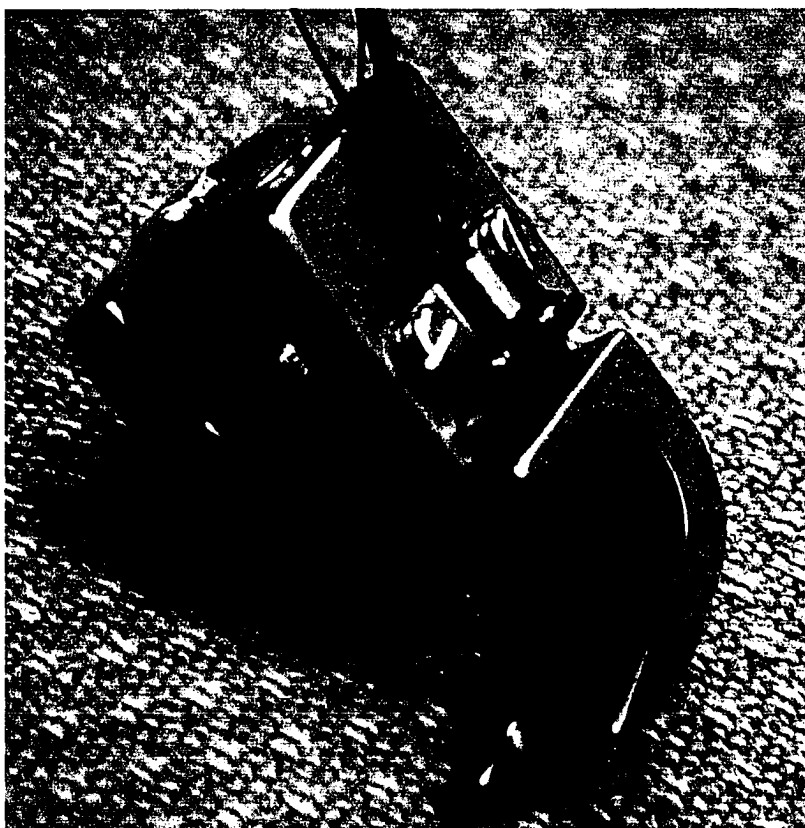


Figure 1.3. A scoliosis hook instrumented with strain gauges. (Photo used with permission of the Glenrose Rehabilitation Hospital.)

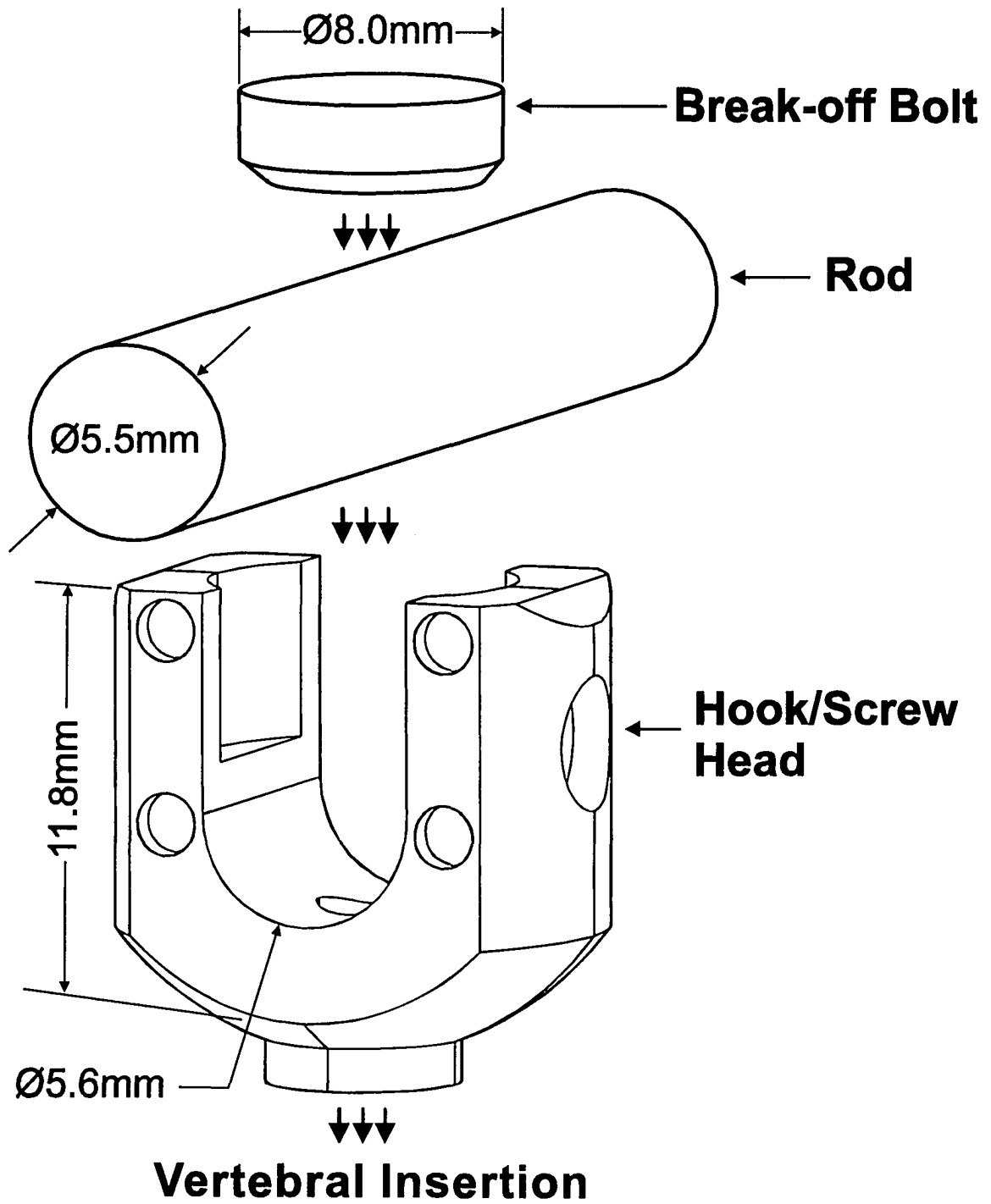


Figure 1.4. Schematic of rod-hook/rod-screw interface.

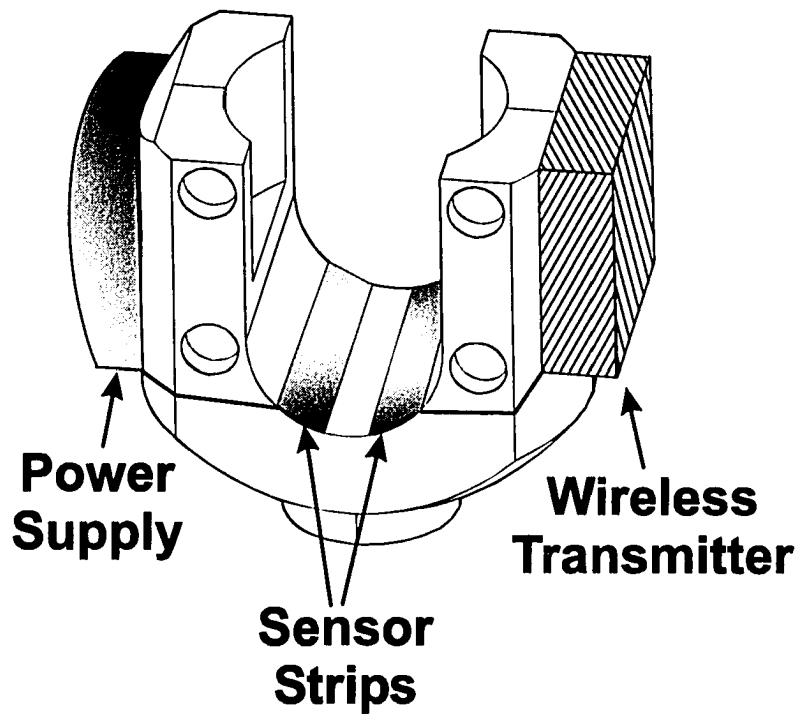


Figure 1.5. Sensor instrumentation attached to the hook or screw head.

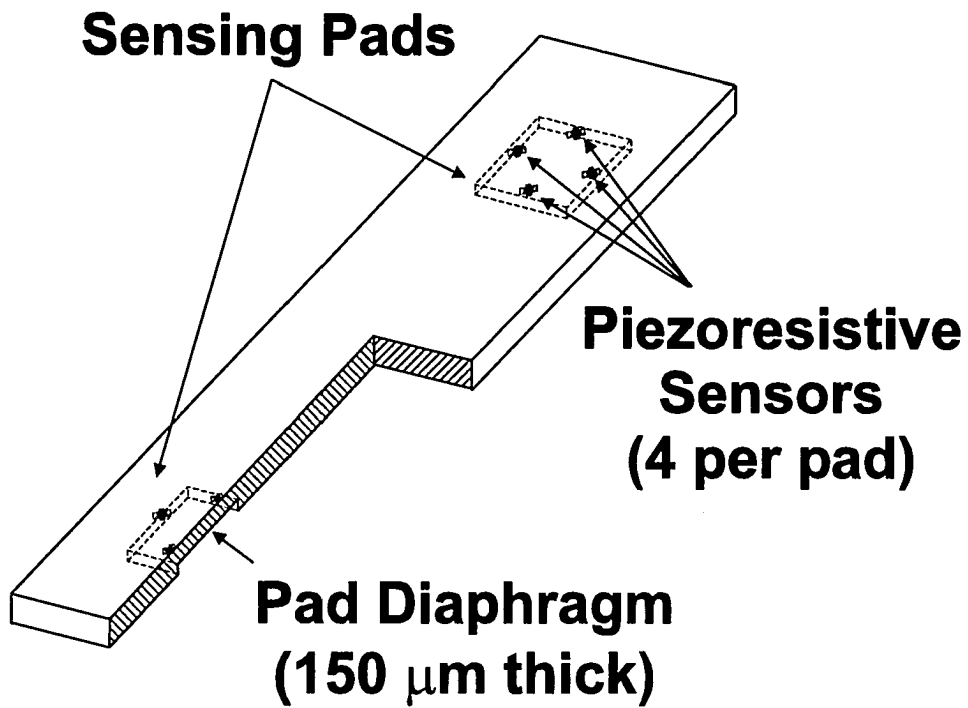


Figure 1.6. Cut-away view of the silicon substrate strip with piezoresistive areas shaded.

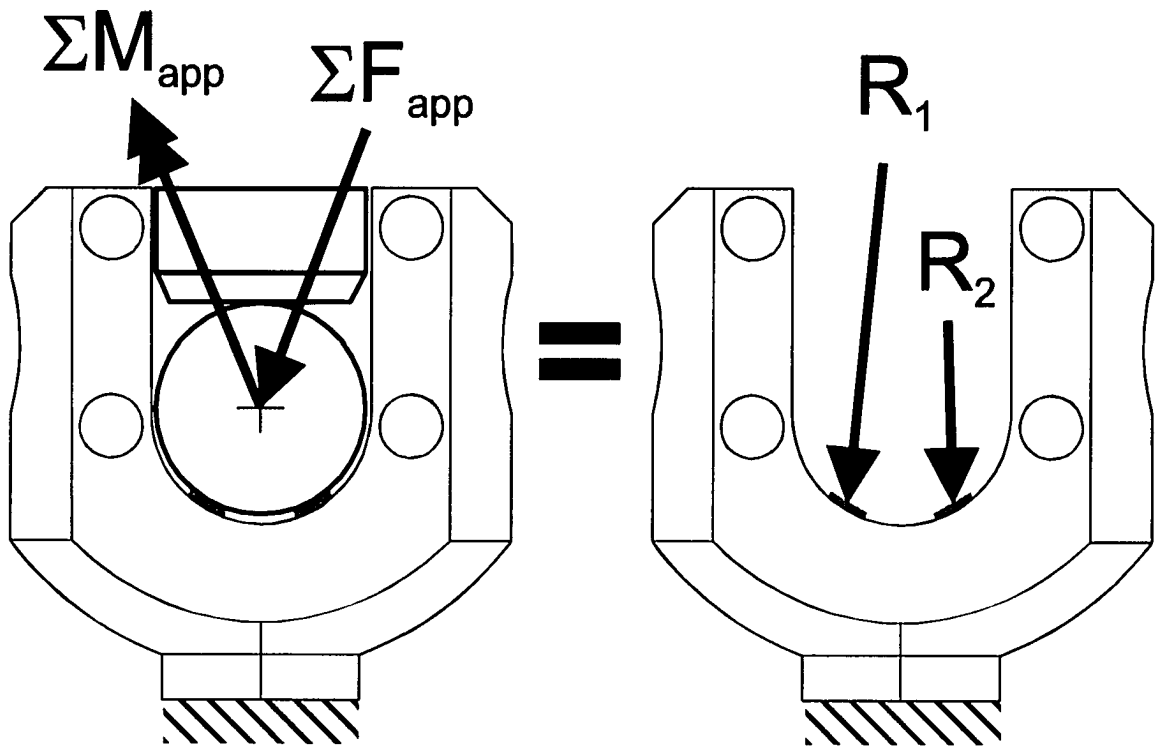


Figure 1.7. Load application on the rod and the equivalent distribution on the sensing strips.

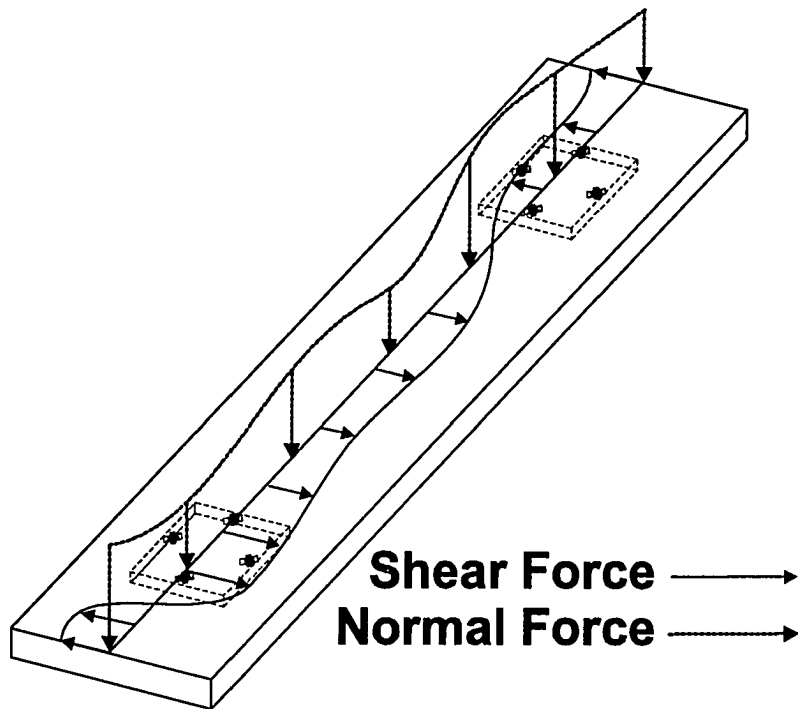


Figure 1.8. Visualization of a load distribution (R_1 or R_2) applied to a sensor strip.

Chapter 2 – Current Technology and Background Information*

The design presented in chapter 1 to measure the three dimensional forces and moments applied during scoliosis correction surgery is justified. A literature review of current, applicable sensor technology is presented to explain the selection of the piezoresistive sensing scheme and why certain features of the sensor were developed. This literature review also explains the general finite element theory used throughout the work. The remainder of the chapter describes the theoretical background of the sensor system, subdivided into sections describing contact, membrane deflection and piezoresistivity. For each of these three subsections, verification of the finite element parameters used in the simulation of the completed sensor system is given.

2.1 – Literature Review of Applicable Technology

A large variety of designs have been reviewed during the development of this sensor system. Rohlmann et al. [8], Najafi and Ludomirsky [17], and Tang et al. [18] have all presented devices with wireless abilities similar to those required for this application, but with sensor components that are not directly usable. Rohlmann et al. constructed a sensor for use in spinal fusion surgery, and while the data collected with their system is applicable, their sensor design is not immediately adaptable to this scoliosis surgery application. Several researchers presented devices of the appropriate size capable of measuring stresses: Lin et al. [19] used a piezoresistive cantilever to measure the contractive forces of a heart cell; Dargahi et al. [20] instrumented an endoscope with a piezoelectric sensor to provide surgical feedback; and Kane et al. [21] implemented an array of suspended membranes with piezoresistors to be used for robotic tactile imaging. Chu et al. [22] presented a capacitive strain sensor capable of measuring material properties. Although these sensors are the correct size for this application, they were found to have load ranges more suitable for microscopic phenomena, making these sensor designs not directly suitable for this application.

Several of the most viable sensor designs were mathematically and numerically modeled to determine if they could be adapted for the higher loads of the scoliosis

* Portions of this chapter have been included in an article submitted to *Sensors and Actuators A*.

surgery application. To accommodate strength constraints, designs employing extended features such as cantilever beams or extruded shear plates were eliminated. High stress concentration factors found at the corners of features have been reported to cause failure strength reductions of up to 95.7% [23]. These concentrations made the extended features prone to brittle failure under the high stresses (overloads exceeding 3000MPa) experienced in this application. Flat-plate diaphragm designs were found to avoid these stress concentration problems and are compatible with a piezoresistive sensing scheme.

Piezoresistive sensors are beneficial in this application for several reasons. They allow linear outputs to be produced, their sensitivity can easily be adjusted by altering the dopant properties and they can be configured to be sensitive to stresses in several directions without an overly complicated design [24]. Several sensors found in the literature [21, 25, 26] were shown to be sensitive to shear and normal stresses from contact loads and have been manufactured with current micromachining technology. The proposed sensor pad is an adaptation of this type of sensor design. Specifically, it has been modified to be slightly larger and is able to accommodate higher contact loads. The four terminal gauge was chosen for the proposed design scheme over a standard piezoresistor because of its inherent temperature compensation and high sensitivity. Other advantages of the four-terminal gauge are simplicity and compactness on the membrane surface, as it does not require the use of a Wheatstone bridge circuit.

2.2 – Finite Element Analysis Theory

2.2.1 – Introduction to FEA

Complex loadings, shapes and materials that are not readily analyzed using conventional methods may be analyzed in a straightforward manner using FEA. In order to simplify their design process, the sensor strips utilized finite element analysis during several different phases of their development. The basic procedure to perform a FEA is as follows: The object to be analyzed is computer modeled, and then is subdivided into simple regions called elements. This discretization process is often referred to as meshing. Material properties (such as mechanical stiffness, electrical resistance and piezoresistivity) are applied to each of the elements in the mesh, and governing relationships such as boundary conditions and element connectivity are defined. This

allows unknowns to be expressed at the corners of elements (these unknowns are typically in the form of displacements for a mechanical analysis). The corners of elements are typically referred to as nodes. By assembling the loads, material properties, governing relationships and unknown values for all elements into a set of equations, a solution can be obtained describing the approximate behavior of the entire object. [27]

2.2.2 – Specification of FEA Parameters

The finite element analyses were performed using ANSYS 8.1 multiphysics software. For the non-electrical components meshed in 3-D, SOLID187 type elements were used. This is a 10-node, tetrahedral, structural solid that is capable of meshing a wide variety of shapes. For 2-D models, the non-electrical components were meshed with PLANE183 elements. The electrical (piezoresistive) components were meshed with tetrahedral SOLID227 elements for the 3-D models and PLANE223 elements for 2-D models. Contact analyses were modeled with surfaces meshed with CONTA174 and TARGE170 elements. Material properties for silicon and steel were found in several places in literature [23, 24, 28, 29]. Silicon was modeled as an orthotropic material with a stiffness tensor having the following coefficients: $c_{11} = 165.7\text{GPa}$, $c_{12} = 63.9\text{GPa}$, $c_{44} = 79.6\text{GPa}$. The piezoresistive (p-type) tensor was defined by $\pi_{11} = 6.5\text{e-}5 / \text{MPa}$, $\pi_{12} = -1.1\text{e-}5 / \text{MPa}$, $\pi_{44} = 138.1\text{e-}5 / \text{MPa}$ and the resistance was defined as $\rho = 7.8\Omega\text{-cm}$. Steel was modeled as an isotropic material with $E = 207\text{GPa}$ and $\nu = 0.3$.

Finite element mesh sizes were varied from trial to trial, and were reduced until convergence with theoretically expected results was achieved. This method of convergence testing required that simplified trials with known solutions be modeled before different sensor designs were tested. Specific values for mesh sizes used are listed with the description of the relevant analysis. Typically, the boundary conditions applied included fixing the displacement of appropriate nodes to zero and applying a zero voltage to other appropriate nodes. Loads were applied as forces or pressures distributed over specified nodes. Once solutions were obtained within the program, post-processing commands were issued to produce usable outputs in both numerical and graphical formats.

2.3 – Contact Analysis Theory

2.3.1 – Contact Theory

The first step in calculating sensor output is to determine the stresses created in the silicon strips as they contact by the rod. Stress distributions created during contact between elastic cylindrical bodies may be predicted with the Hertzian method [30, 31]. This analysis begins by assuming that the cylinders lie parallel to each other and that the contact area is a long, narrow rectangle with dimensions $2b \times l$. The load is evenly distributed along the length of this rectangle (l) and elliptically distributed along the width. The half-width of the contact area (b) will be:

$$b = \sqrt{\frac{2 \cdot F}{\pi \cdot l} \Delta} \quad \text{where } \Delta = \frac{(1-\nu_1^2)/E_1 + (1-\nu_2^2)/E_2}{1/d_1 + 1/d_2} \quad (1)$$

F represents the load between the two cylinders, E , d and ν represent the Young's modulus, diameter and Poisson's ratio of each cylinder, respectively.

The Hertzian formulation is built upon by the Smith-Liu equations [30, 31], which can include shear stresses caused by friction in the contact zone (f represents the coefficient of friction in the following equations). Using the coordinate system defined in Figure 2.1 with b and Δ as defined in (1), the following equations for stresses in elastic bodies are derived:

$$\sigma_x = -\frac{2\nu b}{\pi\Delta} \left\{ z \left(\frac{b^2 + y^2 + z^2}{b} \bar{\Psi} - \frac{\pi}{b} - 2y\psi \right) + f \left[(y^2 - b^2 - z^2)\psi + \frac{\pi y}{b} + (b^2 - y^2 - z^2) \frac{y}{b} \bar{\Psi} \right] \right\} \quad (2)$$

$$\sigma_y = -\frac{b}{\pi\Delta} \left\{ z \left(\frac{b^2 + 2y^2 + 2z^2}{b} \bar{\Psi} - \frac{2\pi}{b} - 3y\psi \right) + f \left[(2y^2 - 2b^2 - 3z^2)\psi + \frac{2\pi y}{b} + 2(b^2 - y^2 - z^2) \frac{y}{b} \bar{\Psi} \right] \right\} \quad (3)$$

$$\sigma_z = -\frac{b}{\pi\Delta} [z(b\bar{\Psi} - y\psi + fz\psi)] \quad (4)$$

These are then combined into Von Mises stresses by the following equation:

$$\sigma_{VM} = \sqrt{\frac{1}{2} [(\sigma_x - \sigma_y)^2 + (\sigma_y - \sigma_z)^2 + (\sigma_z - \sigma_x)^2]} \quad (5)$$

in which,

$$M = \sqrt{(b+y)^2 + z^2}, \quad N = \sqrt{(b-y)^2 + z^2}$$

$$\psi = \frac{\pi(M-N)}{MN\sqrt{2MN + 2y^2 + 2z^2 - 2b^2}}, \quad \bar{\psi} = \frac{\pi(M+N)}{MN\sqrt{2MN + 2y^2 + 2z^2 - 2b^2}}$$

To simulate the sensor-rod contact problem, d_2 was increased to infinity to represent the flat sensor surface and other parameters were adjusted to approximately that of the steel rod ($E_1 = 207$ GPa, $\nu_1 = 0.3$, $d_1 = 5.5$ mm) and the silicon sensor ($E_2 = 120$ GPa, $\nu_2 = 0.28$). F was set to a normal load in the range expected and f was adjusted to reflect the appropriate tangential loading. The outputs from (5) were then used to verify results of a similar contact problem with finite element analysis.

2.3.2 – Contact Simulation

To determine appropriate finite element (FE) parameters for the full hook model several contact problems with known solutions were analyzed. The problems were modeled in two and three dimensions with varying contact parameters. Numerical solutions could then be compared to the analytical solutions provided by the Hertz / Smith-Liu equations (1-5). Figure 2.2 is such a comparison, depicting the Von Mises stress distribution along the contact axis in a solid sensor strip. (The contact axis is defined as the line directly below the contact point, depicted by the z-axis in Figure 2.1). The analysis shown in the figure was performed using 100N of normal and 25N of shear loading applied to a three-dimensional finite element model solved with ANSYS 8.1. It was found that the Von Mises stress levels were very similar with both methods through the majority of the strip; the exception was the region from the contact surface to approximately 50-100 μ m beneath the surface. Finding significant differences between theoretical and numerical results in the region near the surface indicates a potential problem with the calculated reaction loads, so a second verification of the finite element parameters is performed.

The second verification of finite element parameters compares the obtained reaction loads theoretically and numerically in the contact areas. This involves comparing theoretical contact width, defined as b in (1), to the width of the contact area

produced in the numerical analysis. Parameters similar to those used in the previously described Von Mises stress analyses were used as a starting point for comparison of the numerical and analytical contact widths for various mesh sizes. The results of this comparison are illustrated in Figure 2.3. It can be seen that a reasonably accurate (within 3%) numerical contact width is produced when mesh size is reduced to less than half of the theoretical contact width. For this scenario, it was determined that the maximum mesh size is 0.2mm. The final step of this verification is to ensure that conservation of forces was maintained across the contact surface. In addition to establishing appropriate finite element parameters for contact analyses with the sizes and materials used in the full hook model, having an accurate contact width indicates that the reaction loads on the contact surfaces are reasonable.

The purpose of resolving accurate reaction loads on the contact surface is to allow the contact analysis to be separated from the piezoresistance problems. Extracting the equivalent contact forces (R_1 and R_2 , as shown in Figure 1.7) that the rod applies to the sensor pad makes it possible to reduce solution time for the piezoresistive model (used in the final step of the analysis) by up to 90%. The next step of the analysis is the membrane deflection problem, which is included in both the piezoresistive analysis and the contact problems so that the R_1 and R_2 loads are extracted accurately.

2.4 – Description of Square Diaphragm Deformation

2.4.1 – Diaphragm Deflection Theory

This theory has been outlined by Timoshenko [32] for general deflection of a square membrane with all four sides fixed (built-in). This problem represents a very complex application of the theory, as the application from the contact load is generally rectangular with an elliptical force distribution, the plate is anisotropic and irregularly shaped, and the site where the stresses need to be measured is not on an edge or at the center of the plate. This makes the problem well suited for finite element analysis. In order to prove the validity of the finite element routine which is used in both the contact and piezoresistive analyses, a simple fixed membrane problem stressed with a distributed (pressure) load is evaluated. Beginning with the plate equation for small deflections when bending effects are dominant:

$$\nabla^4 w = \frac{p(x,y)}{D} \quad (6)$$

where w is deflection perpendicular to the membrane, $p(x,y)$ is the loading function and D is the flexural rigidity of the plate, or

$$D = \frac{Eh^3}{12(1-\nu^2)} \quad (7)$$

Using the coordinate system as defined in Figure 2.4 it may be derived that:

$$w = \frac{4qa^4}{\pi^5 D} \sum_{m=1,3,5,\dots}^{\infty} \frac{(-1)^{(m-1)/2}}{m^5} \cos \frac{m\pi x}{a} \left(\begin{array}{l} 1 - \frac{\alpha_m \tanh \alpha_m + 2}{2 \cosh \alpha_m} \cosh \frac{m\pi y}{a} \\ + \frac{1}{2 \cosh \alpha_m} \frac{m\pi y}{a} \sinh \frac{m\pi y}{a} \end{array} \right) \quad (8)$$

where q is the magnitude of the distributed load and a is the length of one side of the square plate. This is then modified into equations of the form:

$$\frac{C_i}{i} \left(\tanh \alpha_i + \frac{\alpha_i}{\cosh^2 \alpha_i} \right) + \frac{8i}{\pi} \sum_{m=1,3,5,\dots}^{\infty} \frac{C_m}{m^3} \frac{1}{\left(1 + \frac{i^2}{m^2} \right)^2} = \frac{4qa^2}{\pi^3} \frac{1}{i^4} \left(\frac{\alpha_i}{\cosh^2 \alpha_i} - \tanh \alpha_i \right) \quad (9)$$

with C_i and C_m as series term constants and $\alpha_i = i\pi b/2a$ ($i=1,3,5,\dots$). By substituting numerical values of the coefficients into these equations, a solvable system of linear equations is produced. Table 2.1 (excerpted from [32] for $\nu = 0.3$) shows the results of these systems.

Table 2.1. 'Exact' equations for deflections and bending moments in a uniformly loaded square plate with fixed edges.

$(w)_{x=0,y=0}$	$(M_{xx})_{x=a/2,y=0}$	$(M_{yy})_{x=0,y=a/2}$	$(M_{xx})_{x=0,y=0}$	$(M_{yy})_{x=0,y=0}$
$0.00126qa^4/D$	$-0.0513qa^2$	$-0.0513qa^2$	$0.0231qa^2$	$0.0231qa^2$

Alternatively, approximations given by Westergaard in 1921 [33] as transcribed in [34] are shown in Table 2.2. These equations have a similar form as those shown in Table 2.1, but have different coefficients.

Table 2.2. Westergaard equations for deflections and bending moments in a uniformly loaded square plate with fixed edges.

$(w)_{x=0,y=0}$	$(M_{xx})_{x=a/2,y=0}$	$(M_{yy})_{x=0,y=a/2}$	$(M_{xx})_{x=0,y=0}$	$(M_{yy})_{x=0,y=0}$
$1/525 qa^4/D$	$-1/24 qa^2$	$-1/24 qa^2$	$1/56 qa^2$	$1/56 qa^2$

2.4.2 – Diaphragm Deflection Simulation

A 1mm square silicon membrane was modeled with fixed edges in order to compare the finite element performance of the diaphragm with theory. Isotropic silicon material properties were used in order to better correlate the FE models with the equations derived in section 2.4.1. In various FE trials, pressures were applied to the upper membrane surface and the maximum deformations were recorded. Several membrane thicknesses were analyzed; the results from both the analytical equations (shown in Tables 2.1 and 2.2) and the finite element deflection results were found to be highly linear with q .

Figure 2.5 shows a comparison of the ‘exact’ series solution to a finite element solution for the 1mm square membrane as the membrane thickness is varied. A consistent pressure of 100kPa, isotropic silicon properties, and 25 μ m element edge lengths were used in these analyses. Significant errors are created when the membrane thickness reaches approximately 5% of edge length a (50 μ m for this example). This is to be expected, as this thickness causes stress terms ignored in the derivation of (6-9) to cause errors in the solutions [32, 34]. Element sizes were also varied in this study. Errors due to element sizes were seen to be less significant than errors caused by the membranes being excessively thick. For this model, a 25 μ m element edge length was sufficient to minimize errors in deflection due to the element size. In general, the performance of the FE models is well represented by the equations, provided the general assumptions used in derivation of the equation are consistent with the FE models used.

2.5 – Description of the Piezoresistive Effect

2.5.1 – Piezoresistive Theory for Four-Terminal Gauges

The solution to the contact problem can provide the load distributions R_1 and R_2 on the surface of each sensor strip. These load distributions cause deflection of the membranes which creates a stress-strain distribution in the sensor pads. This stress distribution

affects the electrical resistance of the piezoresistive material and allows each four-terminal gauge to produce an output voltage. Simulating the piezoresistance effect in silicon for a four-terminal gauge [35-37] may be performed according to the procedure laid out in literature [28, 29, 38]. Beginning with the three dimensional form of Ohm's law (t, u, v and w indicate Einstein notation):

$$E'_v = \rho'_{vw} j'_w \quad (10)$$

where E'_v and j'_w are electric field and electric current components in the $0-x'y'z'$ coordinate system ($1 = x', 2 = y', 3 = z'$) as defined in Figure 2.6. ρ'_{vw} are components of the resistivity tensor in the same coordinate system ($11 = x', 22 = y', 33 = z', 12 = x'y', 13 = x'z', 23 = y'z'$).

Since voltage is applied between electrodes 1 and 2 and the sensor is relatively small in the z' direction, it is assumed that j'_1 is the only non-zero component of electric current. This leads to the following relationship between E'_1 and E'_2 :

$$E'_2 = E'_1 \frac{\rho'_{12}}{\rho'_{11}} \quad \text{with} \quad \begin{aligned} V_s &= \int_0^L E'_1 dx' = E'_1 L \\ V_o &= \int_0^W E'_2 dy' = E'_2 W \end{aligned} \quad (11)$$

where V_s is the 3.0V source voltage and V_o is the output voltage (measured between electrodes 3 and 4 on Figure 2.6). Solving for V_o , the equation derived in [36] is reproduced:

$$V_o = \frac{\rho'_{12}}{\rho'_{11}} \frac{W}{L} V_s \quad (12)$$

To solve this equation for the specific stress condition of the problem, ρ'_{11} and ρ'_{12} must be determined. If the stress field is determined by a second order tensor σ'_{vw} and the piezoresistive effect is determined by a fourth order tensor π'_{TUVW} (both of which are normally indexed, the primes indicating that they are in the $0-x'y'z'$ coordinate system), components of the resistivity tensor may be calculated by the following relationship:

$$\rho'_{TU} = \rho_0 \delta_{TU} + \rho_0 \pi'_{TUVW} \sigma'_{vw} \quad (13)$$

where ρ_0 is the resistivity of the unstressed material.

In order to convert stresses and piezoresistive coefficients (associated with silicon orientation) from θ - xyz (global) coordinates to θ - $x'y'z'$ coordinates (orientation of sensor pad) a rotational tensor Q_{VW} may be used. This implies that the equation:

$$r'_{i'} = Q_{VW} r_{iW} \quad (14)$$

is used to convert a first order tensor (where $r'_{i'}$ and r_{iW} are arbitrary first order tensors) and the equation:

$$\sigma'_{TU} = Q_{TV} Q_{UW} \sigma_{VW} \quad (15)$$

is used to convert a second order tensor (stress in this case) to the new coordinate system. To convert the fourth order piezoresistive tensor, the following equation is used:

$$\pi'_{TUVW} = Q_{TP} Q_{UQ} Q_{VR} Q_{WS} \pi_{PQRS} \quad (16)$$

The stress state (σ_{TU}), piezoresistive matrix (π_{TUVW}), direction cosines (Q_{VW}), unstressed resistivity (ρ_0) and source voltage (V_S) may be used with (12-16) to solve for the output voltage (V_O) produced by a four-terminal sensor under any stress state.

2.5.2 – Simulation of the Four Terminal Gauge

To verify the finite element simulation of a four-terminal gauge, a simply supported model is built to allow the application of a simple stress state. The stress state examined can be depicted in matrix form by the following equation:

$$[\sigma] = \begin{bmatrix} \sigma_x & 0 & 0 \\ 0 & 0 & 0 \\ 0 & 0 & 0 \end{bmatrix} \quad (17)$$

A simple model similar to an example in the ANSYS help file [29] allows a straightforward comparison to be made between the numerical simulation of a piezoresistive sensor and the analytical solution derived in section 2.5.1.

A three-dimensional model of a four-terminal sensor is built, and the stress state shown in (17) is uniformly applied. Comparing the output voltages obtained with the FE model to theoretical values determined using (12-16), it has been shown in several analyses that outputs are dependent on several parameters. For a p-type silicon device on the (100) plane, maximum sensitivity is achieved when the x -axis is aligned with the $\langle 110 \rangle$ direction and terminals 1 and 2 (x' -axis) of the four terminal gauge are at a 45°

angle to the applied stress. Numerical and theoretical solutions for normalized sensitivity of a four-terminal gauge with stress applied in the $\langle 110 \rangle$ direction is plotted as the x' -axis of the gauge is rotated in Figure 2.7. Modifying the relative geometry of the sensor (adjusting the W to L ratio) determines that the optimum value is 1:2. Both of these values for variable optimization are well supported in the literature [28, 29, 35-38] and have been observed for the finite element trials performed. Values for x -axis, x' -axis, W , L , terminals 1 and 2 are described in section 2.5.1 and shown in Figure 2.6.

Finite element mesh size is another parameter that affects the performance of the numerical simulation. To examine this effect, the numerical zero load voltage is compared to the theoretical zero as the mesh size is varied. Ideally, the zero-load voltage should be zero in all cases, but this is not observed experimentally. Figure 2.8 shows that the numerical zero-load voltage approaches zero as the mesh size is decreased. This analysis indicates that for the piezoresistive areas a mesh size below $10\mu\text{m}$ will achieve reasonably low errors in output voltage.

Utilizing appropriate FEA parameters obtained from the above verification trials, a model of the entire hook body and sensor strips (without piezoresistive features) may be created. A normal load is then applied to the rod to simulate tightening of the break-off bolt, and then the simulated external load can be applied. This model will then produce load distributions R_1 and R_2 on the strips, which consist of normal and shear force distributions along the length of the strips. These values can then be transferred to a second FE model optimized for piezoresistive analysis, where the final output voltages can be obtained.

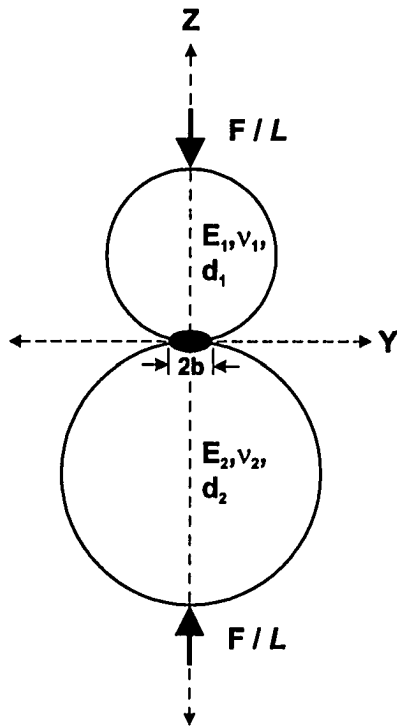


Figure 2.1. Schematic of elastic cylinder contact for the Hertz and Smith-Liu equations.

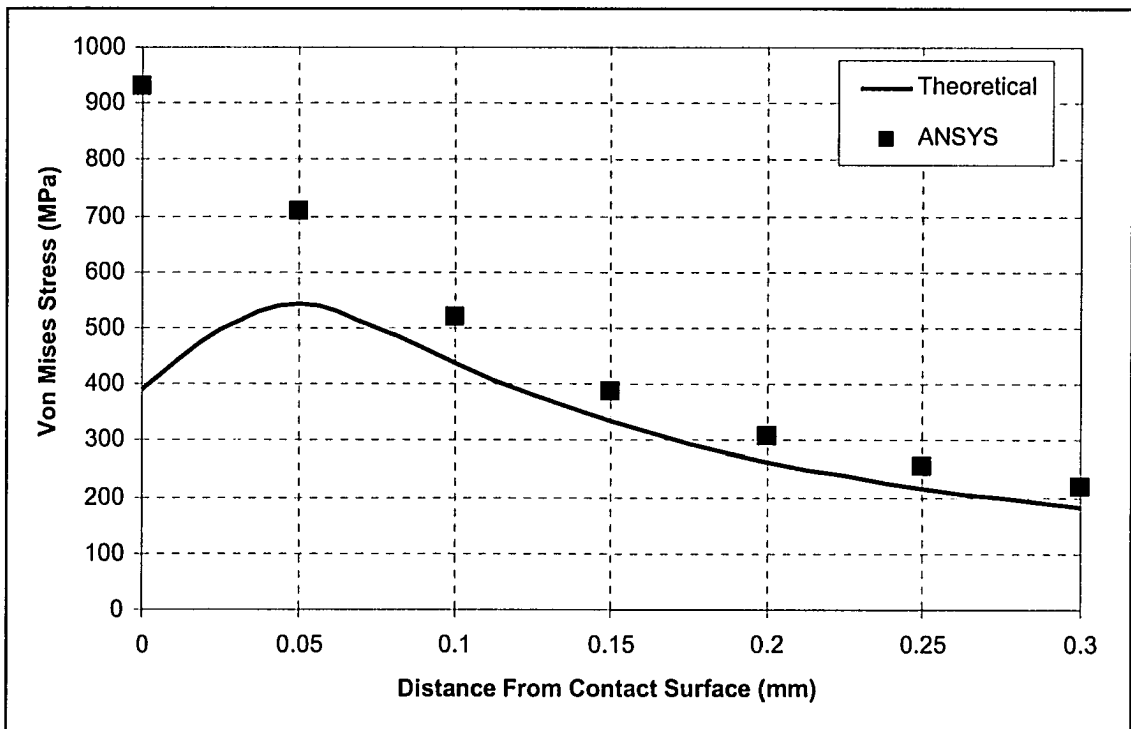


Figure 2.2. A comparison of numerical and analytical stress distributions in a sensor strip.

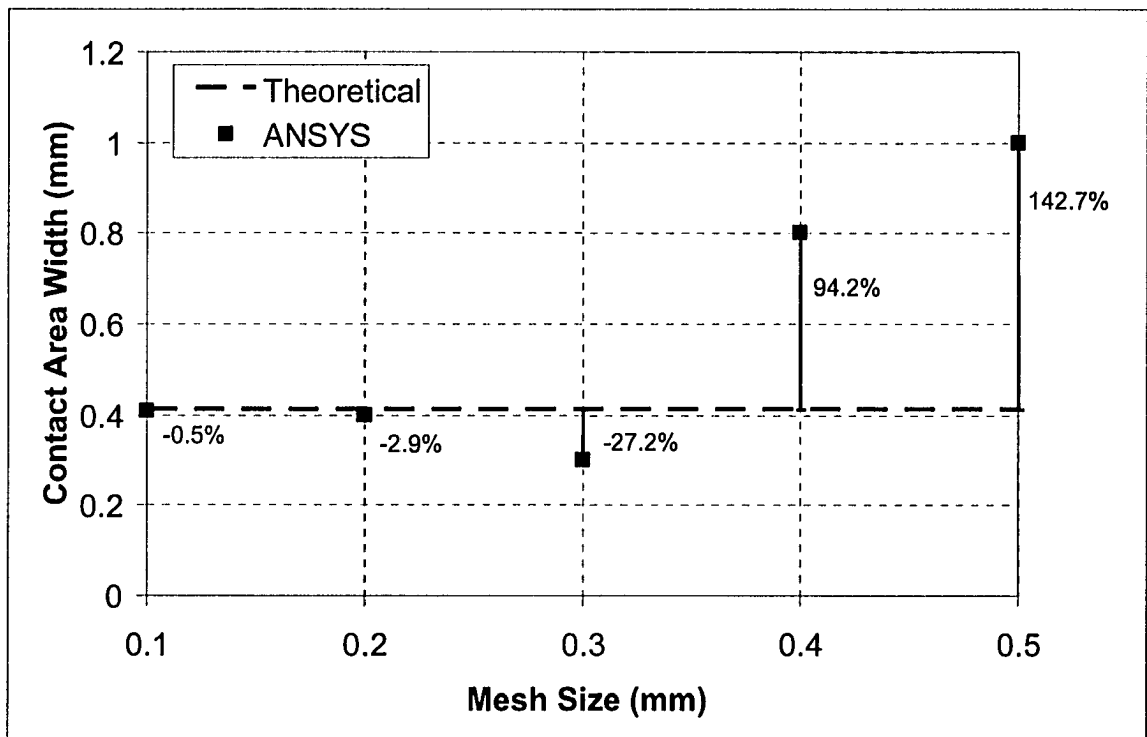


Figure 2.3. Error calculation for numerical contact width as a function of mesh size.

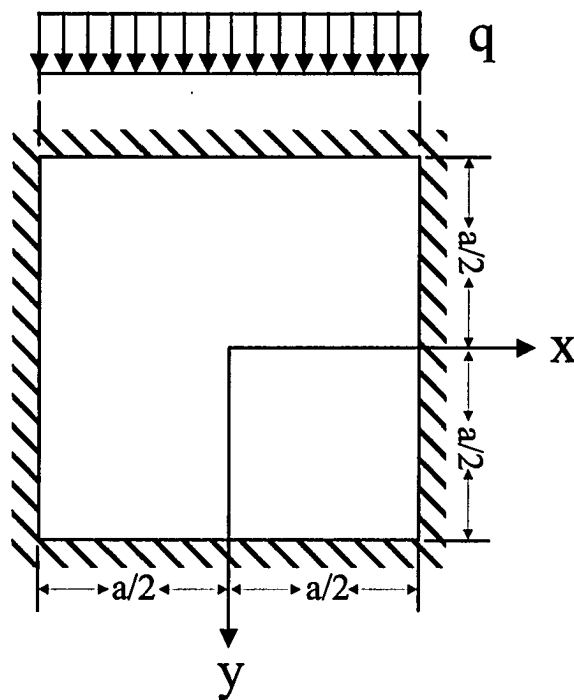


Figure 2.4. Coordinate system used for derivation of membrane equations.

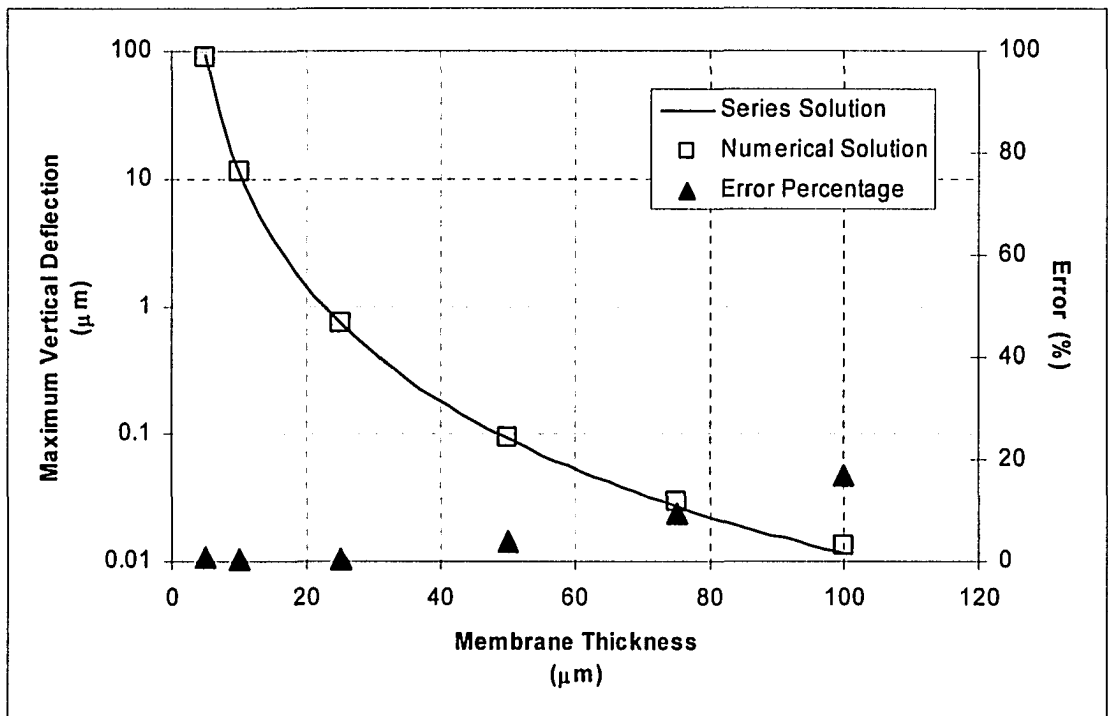


Figure 2.5. Comparison of theoretical and numerical membrane deflection for a 1mm square membrane under a 100kPa pressure load.

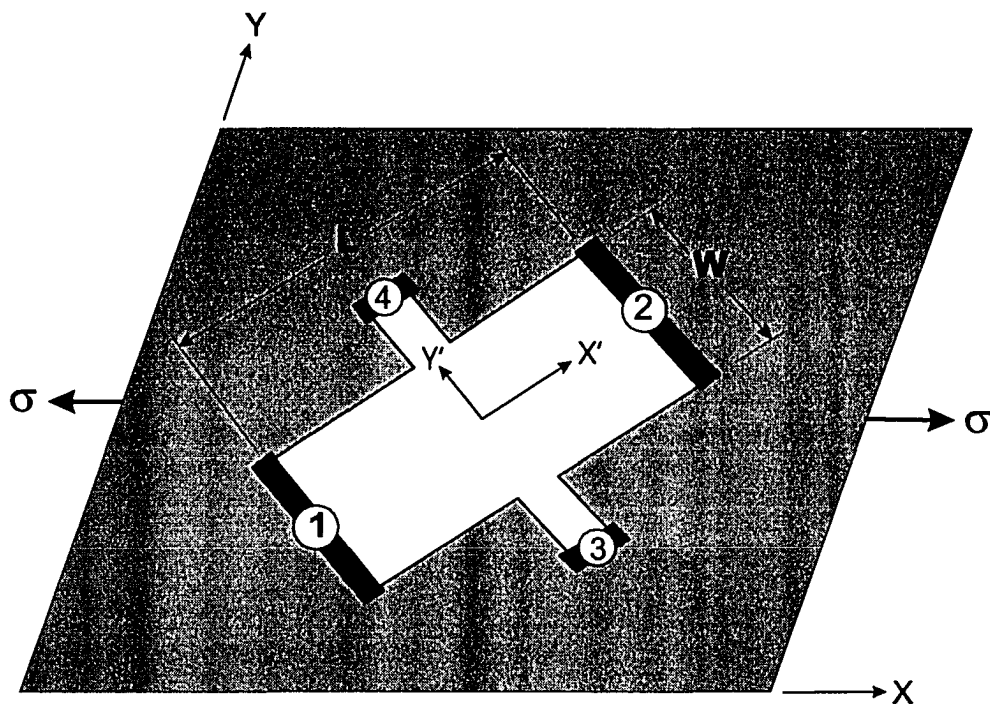


Figure 2.6. Schematic of the four-terminal gauge.

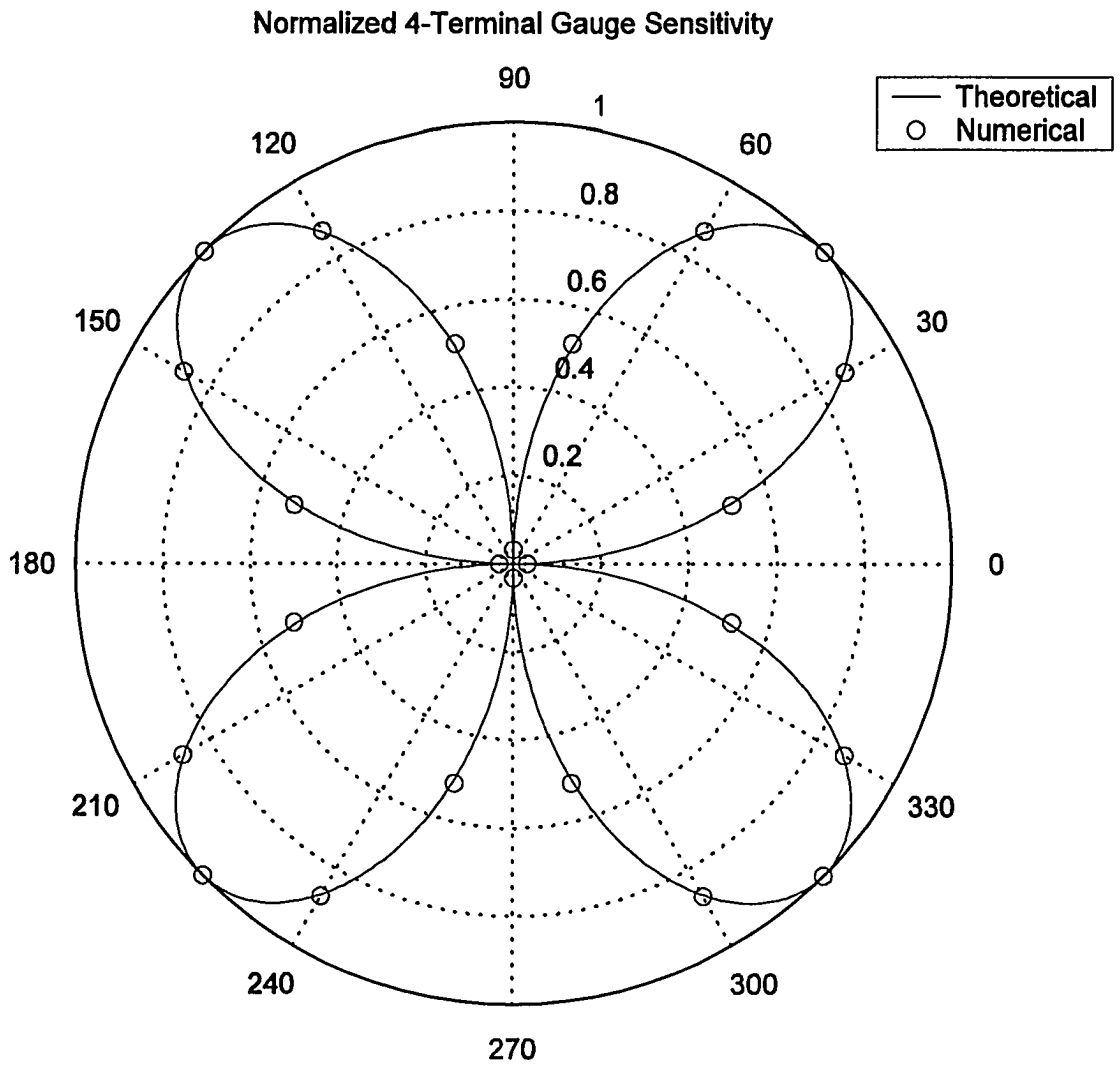


Figure 2.7. Sensitivity of the four-terminal gauge as it is rotated (see text for explanation).

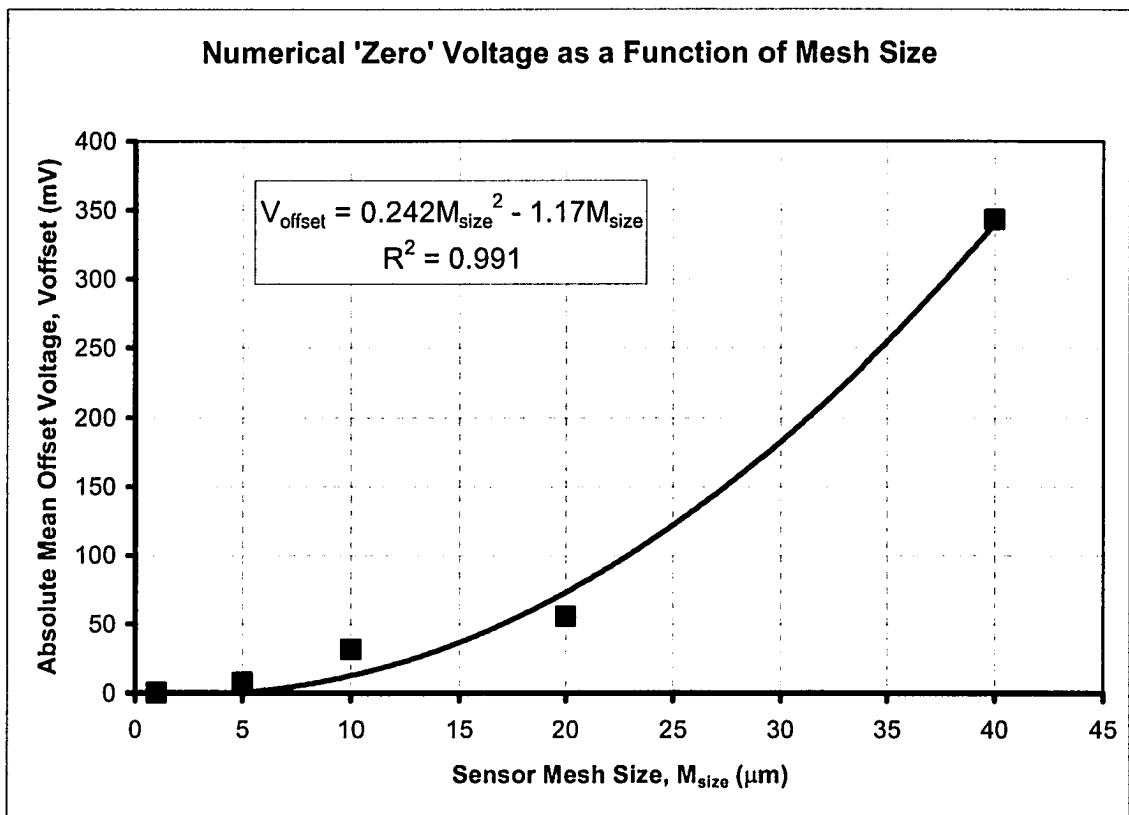


Figure 2.8. Zero voltage as a function of mesh size.

Chapter 3 – Description and Proof for the Proposed Sensor

Several specifics of the sensor design which have not been previously described will be outlined in greater detail in this chapter. Features specified include the location and orientation of the sensor strips in the hook or screw notch, as well as the layout of pads and piezoresistors on each strip. The sensor design is proven in a simulated normal loading scenario, subdivided into a contact analysis and a piezoresistive analysis. Sensitivity results from this analysis are then used to create equations to resolve normal forces from the voltage outputs.

3.1 – Detailed Device Description

3.1.1 – Layout Overview

The general layout of the sensor has been determined by the constraints given, but several details of the design were variables that were experimented with before they were decided upon. Specifically, the orientation of the sensor strips within the hook notch must be chosen, the pads must be placed on each strip and the piezoresistive sensors must be placed on each pad. In addition, appropriate dimensions for the membranes and piezoresistors need to be chosen. Methodology for making these choices is described below from the top down: strips, pads, piezoresistive sensors.

3.1.2 – Strip Placement

The decision to place the sensors on strips within the hook or screw notch was made to minimize the structural modifications to the hook or screw necessary to add instrumentation. This design only requires adding material to the hooks and screws, which does not weaken their structure or make them less functional than unmodified hooks or screws. Another added advantage is not being required to re-machine any standard hook or screw components while building the sensor, which can be expensive and time consuming. Angling two strips toward each other in the notch is an effective technique to resolve three-dimensional forces and moments; the 30° orientation reduces tangential forces from the preload (normal force) while allowing for adequate separation between the two strips. Reducing tangential forces produces lower, safer overall stress

levels in the strips and adequate separation of the two sensors is a factor in resolving forces and moments in multiple directions. Figure 3.1 shows a cutaway view of the placement of a strip within a hook notch.

3.1.3 – Pad Placement

The number and location of membrane pads on each strip were specified to allow three dimensional forces and moments to be resolved. Once it was decided that there would be two strips within each hook or screw notch, a contact analysis of the notch area with solid strips inserted was performed. By evaluating the stress distributions on the surfaces of the strips during the application of three dimensional forces and moments, it became possible to see where the optimum pad sites lay. In all loadings, the stresses were distributed along the long-axis mid-line of the strips, directly under the contact line with the rod. This made placing the pads along these mid-lines necessary.

The contact analysis also determined that during certain moment loading scenarios, one end of the strip was loaded differently than the opposite end. This implied that there should be two pads along the mid-line of each strip, located as far away from each other as possible to maximize the difference in their stress distributions, i.e., to maximize their sensitivity to moment loads. Despite this finding, it was not practical to place the pads right at the ends of the strips since stress concentration sites were found at these locations during all loading scenarios. These concentration sites were undesirable locations for the membranes due to their extreme stress magnitudes and comparative inability to resolve differences in loadings. To adequately isolate the pads from these stress concentration sites, a distance of 1mm from the ends of the sensor to the center of the pad was used, as this distance was found to be in the appropriate stress region. The locations of the pads (shown in black) on a sensor strip are shown in Figure 3.1.

3.1.4 – Membrane Details and Piezoresistive Sensor Placement

To quantify the dimensions of the membranes and the piezoresistive sensors placed on them, several finite element models of silicon membranes were built. The FE models were simplified to be square sections of anisotropic silicon substrate with a square membrane located in the middle. The external dimensions of this section are 1.5mm x

1.5mm x 0.5mm; the large dimension is representative of the chosen width of the strip, and the small dimension is the approximate thickness of the silicon substrates available. The truncation of the strip's length was found not to affect the model's performance as loads applied further away from the pads and sensors do not have a significant effect on the local stress distribution. Dimensions of the square membrane could be adjusted to experiment with different thicknesses and edge lengths. Four piezoresistive sensors were placed on the surface of this membrane in configurations that could be adjusted. For simplicity, the dimensions of the individual piezoresistors were fixed at $W=50\text{mm}$ and $L=100\text{mm}$, with a source voltage across terminals 1 and 2 of 3.0V (see section 2.5 for explanation of piezoresistive terminology). The loads applied to this model were in the form of a load distributed over a rectangular area as described by theoretical contact equations (see section 2.3). Finally, the bottom surface of the substrate was fully constrained to provide a structural boundary condition. A schematic of this model is shown in Figure 3.2.

A stress analysis was performed on the simplified membrane model to determine the appropriate thickness and edge length for the membrane. The model used in this FEA did not incorporate any piezoresistive elements, and could be solved quickly for Von Mises stress distribution using an element size of $50\mu\text{m}$. This determined that the most highly stressed area of the membrane is the mid-point of the edges on the top or bottom surfaces. Membrane theory also supports this finding [32]. Provided that the sensors do not have large stress concentration sites on the underside of the membrane, stress analysis shows that a membrane thickness of $150\mu\text{m}$ and an edge length of $750\mu\text{m}$ are appropriate dimensions to avoid failure of the silicon with the loads experienced in this application.

The location where the highest stresses occur in the membranes is also the ideal location for the piezoresistive sensors to be placed. This specifies that the four piezoresistive sensors should be located on the top surface of the sensor above the center of each of the four membrane edges. Calculation of the electrical outputs in this model also influences placement of the membrane. Initially, the edges of the membrane were aligned with the edges of the substrate on this model (as shown in Figure 3.2). This places two of the piezoresistive sensors directly underneath the rod, causing large, localized stress distributions at these two sensor areas where the rod directly contacts

their top surfaces. Therefore, electrical outputs from these sensors are not available for this simulation, which makes sensor characterization difficult. When the actual sensor is manufactured, it is assumed this stress localization will be less pronounced due to load distribution over a continuous area rather than individual nodes, and the epoxy sealant on the pad surface should aid in minimizing concentration effects. However, since this concentration effect may still be problematic in the manufactured sensor, this effect is eliminated by rotating the membrane pads and sensors by 45°, which creates a gap between the rod contact site and the piezoresistive area. The rotated model is shown in Figure 3.3, and uses the same rotational configuration of the sensors used in the device trials.

3.2 – Contact Loading Applied in the Normal Loading Scenario

3.2.1 – Device Symmetry and Finite Element Modeling

This device can be shown to be symmetrical about two planes when under a loading scenario that is purely normal. These planes of symmetry and an indication of the normal force direction are shown in Figure 3.4. A finite element model consistent with the quarter-model shown in this figure is built, and a 250N normal load (one-quarter of the maximum normal load expected on this device) is applied. The bottom surface of the FE model is constrained to simulate fixation to the spine with either a hook or screw. The contact surfaces (the sensor pad and rod) are meshed with 250µm elements, which is less than half of the theoretical contact width for the model under the applied load. This element sizing is necessary to produce accurate results with this contact analysis (this is described in greater detail in section 2.3.2). However, 250µm element sizing is still considerably (approximately ten times) larger than the sizing necessary for the piezoresistive analysis to produce accurate results. By separating the contact and piezoresistive problems, larger elements can be used in the contact analysis. This was found to decrease total solution time very effectively. The fully defined contact problem was then solved numerically.

3.2.2 – Calculated Contact Loads

The solution to the contact problem can be examined to extract the reaction forces (a portion of R_1 or R_2) applied to the membrane. In order to make this solution useful for the piezoresistive analysis, the spatial coordinates and three-dimensional force information for each node with a contact reaction are stored. The finer mesh size used in the piezoresistive model necessitates distributing each of these forces over several points when the loads are re-applied. In the piezoresistive model, several load magnitudes should be applied in order to calibrate the sensors. Conveniently, the results of the contact analysis are automatically broken down into several load steps as the solution is calculated. At each of these load steps contact force information may be stored for re-application into the piezoresistive problem.

The displacement of the sensor pad caused by the reaction forces is shown in Figure 3.5. The maximum displacement in the quarter model occurs above the membrane. This location also corresponds to the lowest contact pressure, which is shown for the rod in Figure 3.6. Lower contact pressure on the membrane logically follows from the membrane area having a lower stiffness than the solid portion of the silicon strip; the relatively compliant membrane cannot resist the rod's displacement as strongly as the rest of the strip.

3.3 – Numerical Evaluation of Output Voltages

3.3.1 – Piezoresistive Sub-Model

Load distributions and appropriate piezoresistive parameters have been determined in sections 3.2.2 and 2.5.2, respectively. Using these values, output voltages for the 4-terminal sensors as attached to the hooks can be calculated. For this phase of the analysis, a half-strip model containing only one pad (as shown in Figure 3.7) was created. This model is similar to the strip on the quarter-hook used as part of the model in the preceding section (this model is shown in Figure 3.4). A $150\mu\text{m}$ membrane with $750\mu\text{m}$ edge lengths is created on the midline of a $4150\mu\text{m} \times 1500\mu\text{m} \times 500\mu\text{m}$ sensor pad, approximately $1000\mu\text{m}$ from one end. Instead of modeling the entire quarter hook/screw body as was done in the previous section, a $500\mu\text{m}$ steel base was added below the silicon strip and the bottom surface of this base was fully constrained. This

simplification significantly reduced the number of elements and solution time. Simplifying the piezoresistive analysis model was also found to have a minimum impact on the reaction forces occurring on the bottom surface of the silicon strip and did not significantly change the stress distribution in the compliant membrane pad. A potential difference of 3.0V was applied to the appropriate terminals on each piezoresistive sensor and the model was solved to obtain output voltages.

3.3.2 – Calculated Voltage Outputs

Surface loads equivalent to full-hook normal forces varying from 0 to 1000N were applied to the piezoresistive model. Output signals (in the form of voltages) were collected from each piezoresistive area for each load applied. The simulated outputs for the rotated-pad model are shown in Figure 3.8. These quarter-model FEA results can be used to specify operation of the complete system. Model symmetry for the normal load scenario, as described in section 3.2, dictates that the 16 outputs from the complete system will be made up of four sets of four signals similar to those produced in the quarter-model trials shown. For load scenarios other than the normal case, model symmetry may not apply and the previous analyses must be adjusted accordingly. The 16 output signals sent allow calculation of the device's sensitivity in the various loading scenarios. Using these sensitivity values, equations can be obtained that will allow output signals to be converted back into force values during load application.

3.3.3 – Sensor Pad Calibration Equations

Re-examining the quarter-model results, it is seen that the outputs from all four-terminal sensors are similar in magnitude and distribution shape, and may be fit with a high degree of accuracy ($R^2 > 0.99$) by quadratic trend lines. The outputs from each four-terminal sensor on the pad are not all identical (nor do they have identical absolute values). This is due to the 30° angle that the sensor strips make with the hook or screw notch, which causes a normal load applied to the rod to impart both normal and tangential loads to the surface of the strip. For example, the FEA described in section 3.2 reveals that a 250N normal load applied to the rod produces loads normal and tangential to the strip of 258N and 53N, respectively (loads along the axis of the notch are approximately zero in this

case). Each of the four piezoresistors on each sensor pad has a specific sensitivity to normal and tangential loads which, depending on the location of the sensor on the pad, may have an additive or subtractive effect on total voltage output.

A simple case is used to illustrate the calibration procedure. Loads are applied relative to a strip in three directions: the normal direction, S_{nor} , aligned with the 258N load from the previous analysis, the tangential direction, S_{tan} , aligned with the 53N load and the axial direction, S_{axl} , aligned with the axis of the notch. The strip model used is similar to the piezoresistive model described in section 3.3.1, although certain dimensions are not consistent with those used in the actual design. Using the exact dimensions of the sensor pad is not essential for calibration at this phase of the analysis, due to the fact that rod misalignment and manufacturing variances will likely effect sensor performance enough to warrant individual calibrations of the manufactured devices.

Separate loads are applied in each of the three load directions and approximate sensitivities are calculated by linear curve fit. (Accuracy of this analysis may be improved by using a quadratic equation or stored calibration curves to convert voltages back to applied forces. Linear sensitivity is used here for clarity.) These sensitivities are shown in Table 3.1

Table 3.1. Sensitivities of a test pad under shear and normal loading.

Sensor	Normal Sensitivity (mV/N)	Tangential Sensitivity (mV/N)	Axial Sensitivity (mV/N)
V1	$M_{N1} = 1.593$	$M_{T1} = -0.160$	$M_{A1} = -0.896$
V2	$M_{N2} = -1.582$	$M_{T2} = -0.169$	$M_{A2} = 0.906$
V3	$M_{N3} = -1.534$	$M_{T3} = 0.082$	$M_{A3} = -0.824$
V4	$M_{N4} = 1.545$	$M_{T4} = 0.086$	$M_{A4} = 0.818$

It is assumed that the values of the sensitivities will vary once the devices are manufactured, but their general trends should be consistent (i.e. positive and negative signs will remain constant, and similar values will remain similar). With this information, solving for local strip forces can be performed with the following equations:

$$S_{nor} \cong \left(\frac{V1}{M_{N1}} + \frac{V2}{M_{N2}} + \frac{V3}{M_{N3}} + \frac{V4}{M_{N4}} \right) / 4 \quad (18)$$

$$S_{tan} \cong \left(\frac{V1}{M_{T1}} + \frac{V2}{M_{T2}} + \frac{V3}{M_{T3}} + \frac{V4}{M_{T4}} \right) / 4 \quad (19)$$

$$S_{axl} \cong \left(\frac{V1}{M_{A1}} + \frac{V2}{M_{A2}} + \frac{V3}{M_{A3}} + \frac{V4}{M_{A4}} \right) / 4 \quad (20)$$

Testing these equations with a combined loading of 125N normal, -25N tangential and 0N of axial load, the original forces may be resolved from output voltages alone. With this loading, the finite element analysis produces the following output voltages: $V1 = 191.4\text{mV}$, $V2 = -199.1\text{mV}$, $V3 = -187.2\text{mV}$ and $V4 = 192.2\text{mV}$. Inputting these four voltages back into (18-20) will produce $S_{nor} = 123.1\text{N}$, $S_{tan} = -20.1\text{N}$ and $S_{axl} = 7.2\text{N}$. The S_{nor} value has an error of 1.9N, the S_{tan} value has an error of 4.9N and S_{axl} simply differs from zero by its value. Despite the inaccuracy of the linear equations, these error values are quite reasonable. Assuming a range of 1000N and a 10bit A/D converter with 3.0V excitation, this trial produces a maximum full-scale (FS) error of 0.72% and has a minimum accuracy of $\pm 3.6\%$ FS for tangential loading.

Once the loads local to each pad are known, it is possible to determine the magnitude of the normal load applied to the rod. Since it has been shown that a normal load produces an $S_{nor}:S_{tan}:S_{axl}$ ratio of approximately 5:1:0 for all four pads, equations using the local loads on each pad can be set up to determine the normal loads applied to the rod. The specific form that this normal equation takes, as well forms for equations to calculate the other five loads that may be applied to the rod, is specified in the next chapter. When each hook or screw is calibrated these six equations are what make it possible to resolve forces and moments in three dimensions.

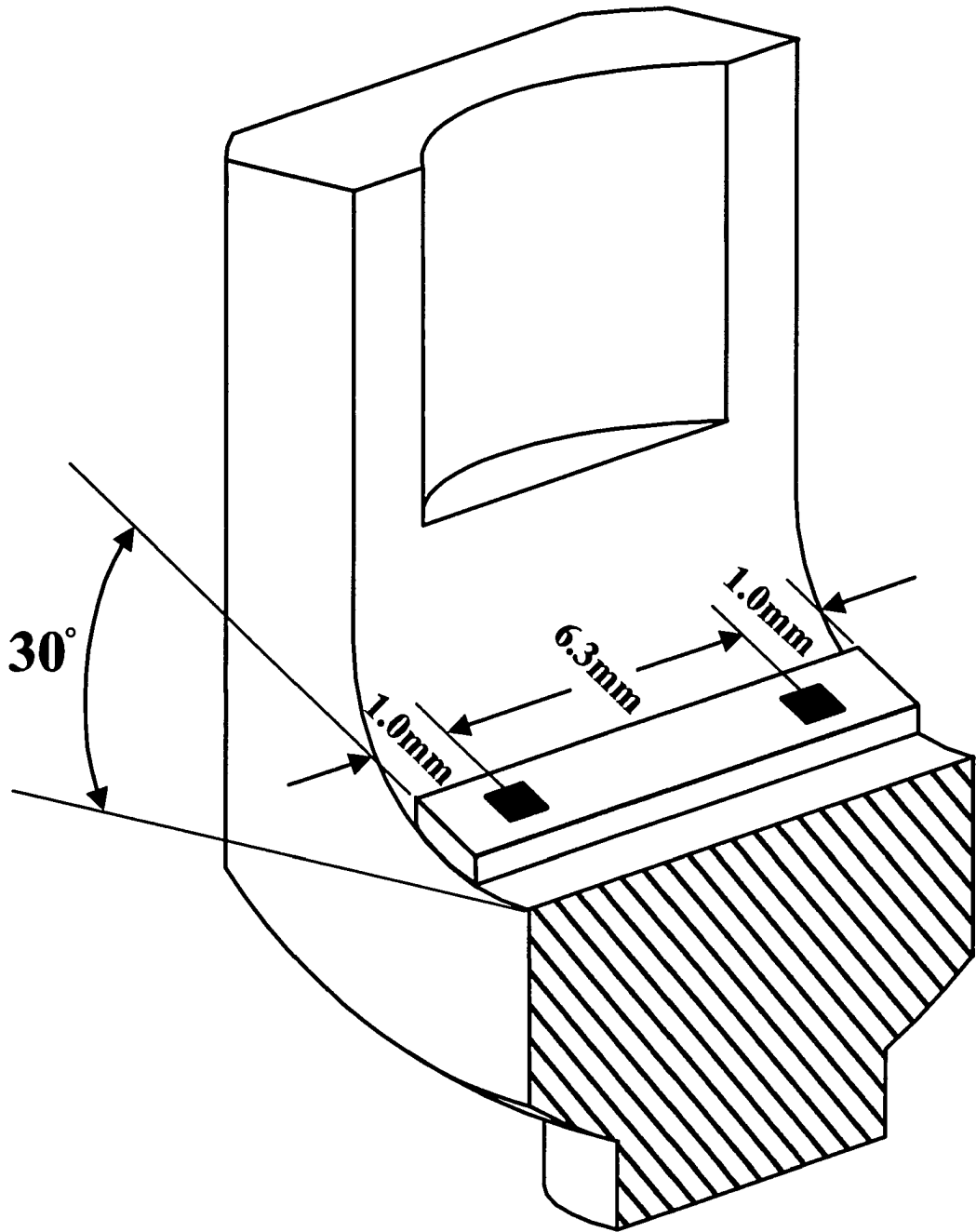


Figure 3.1. Cutaway view of the sensor strip in a hook notch.

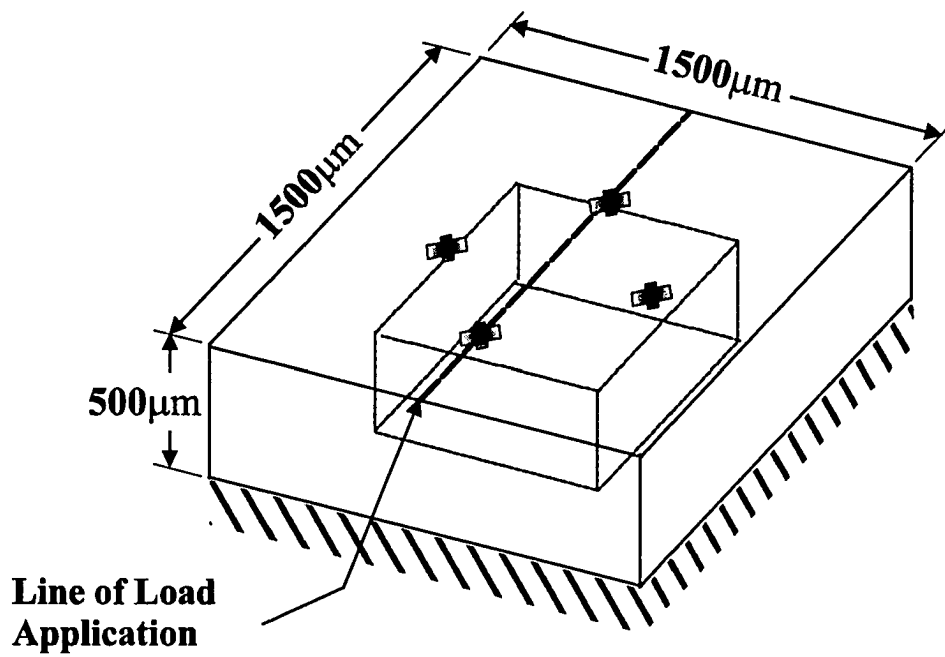


Figure 3.2. Membrane sensor numerical test model.

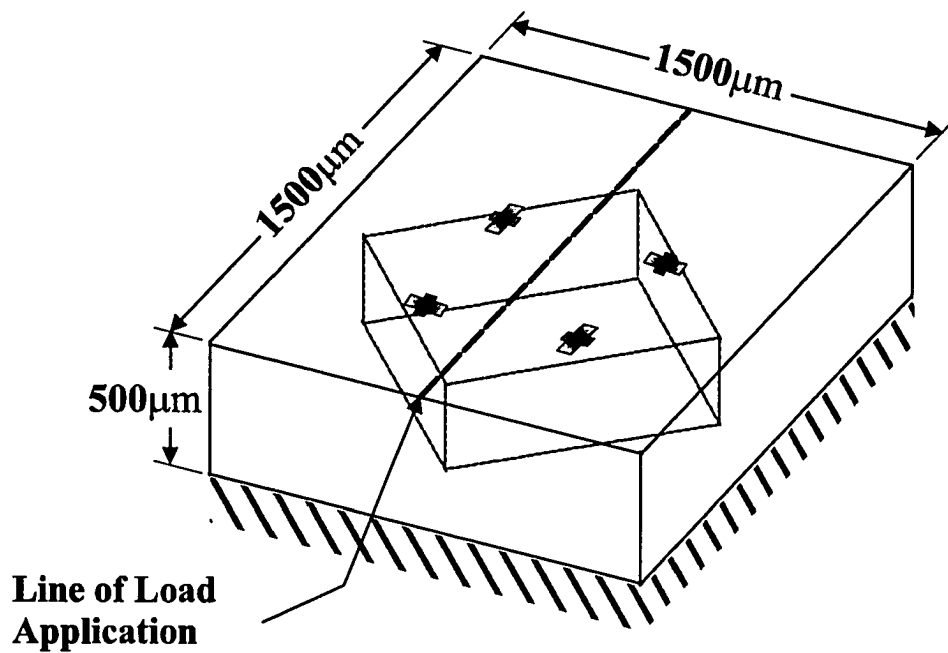


Figure 3.3. Rotated membrane sensor numerical test model.

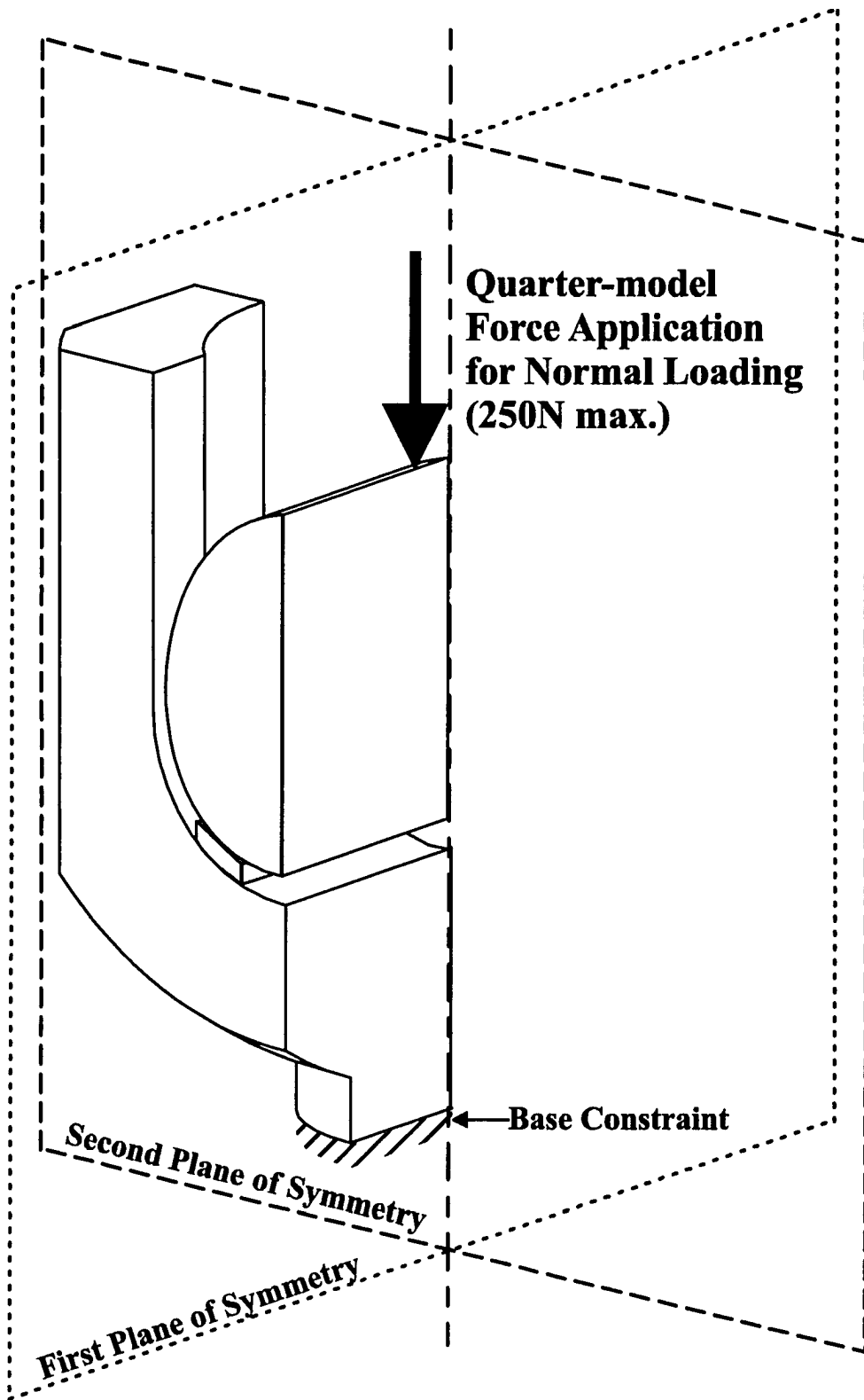


Figure 3.4. Hook/screw model used for normal loading contact analyses with planes of symmetry shown.

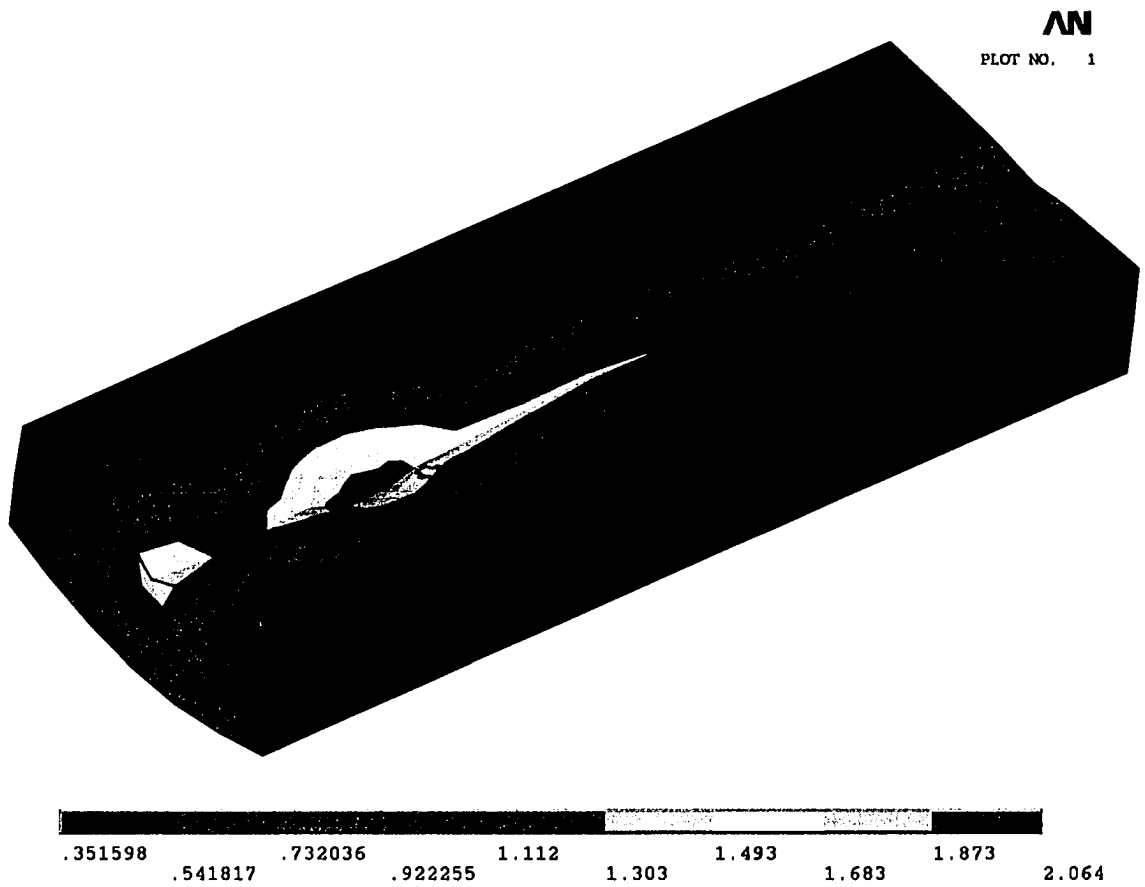


Figure 3.5. Numerical results for membrane deformation (μm units).

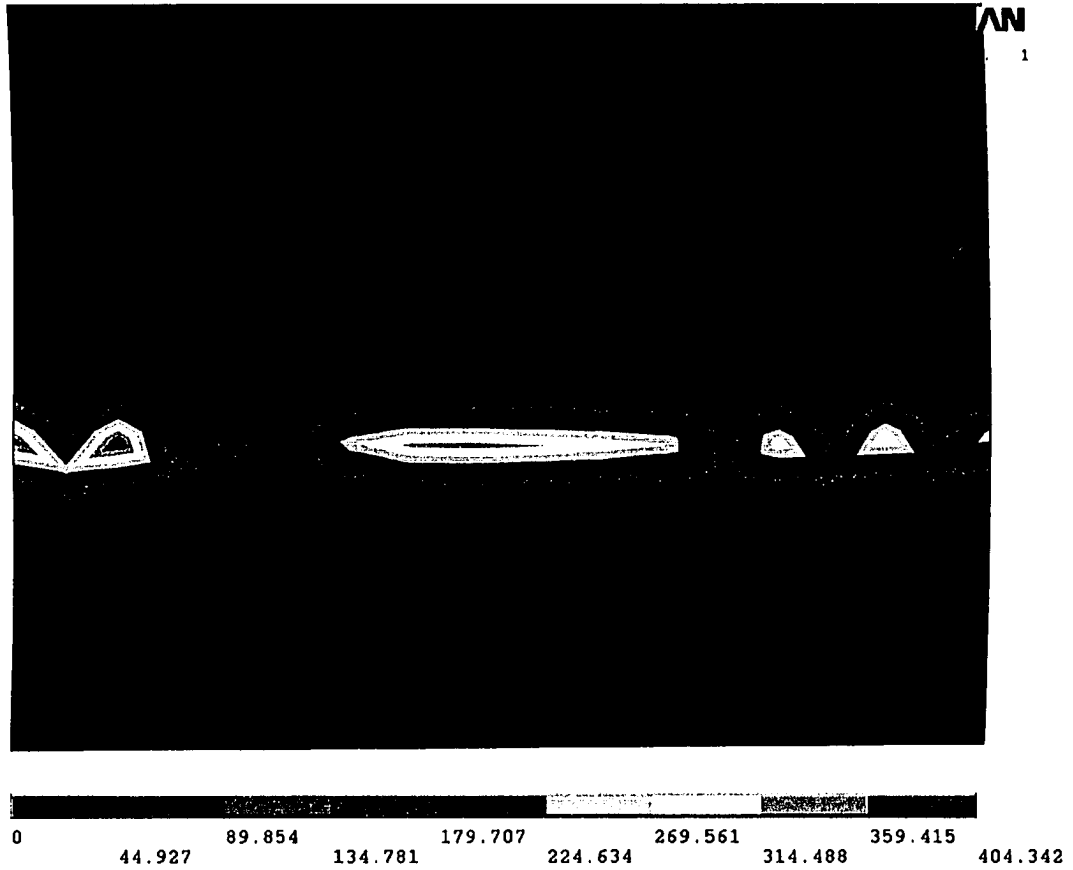


Figure 3.6. Numerical results for contact pressure on the rod (MPa units).

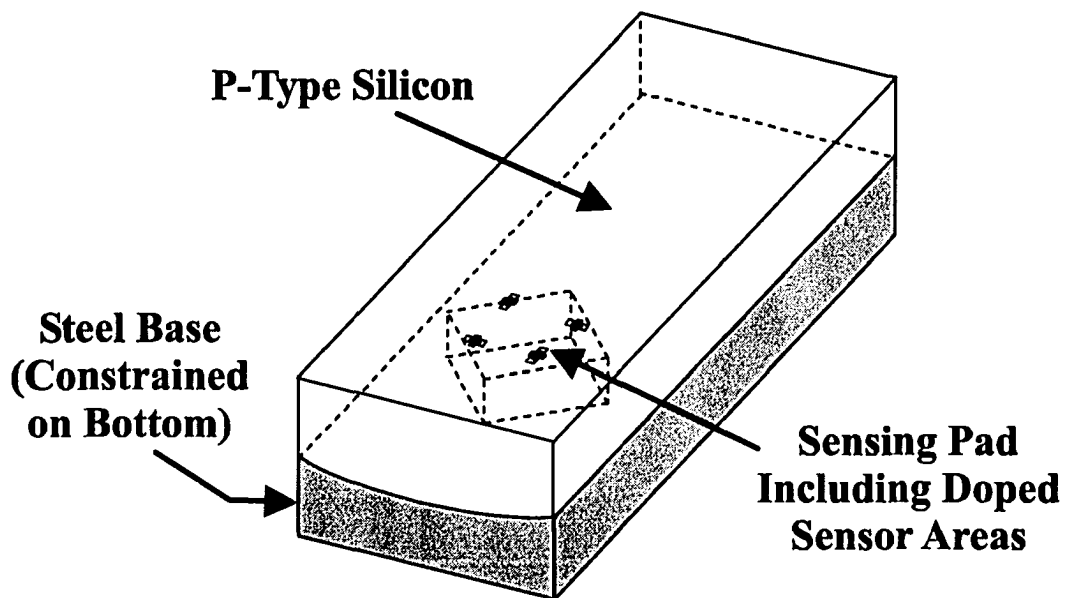


Figure 3.7. Half strip model used for piezoresistive analysis.

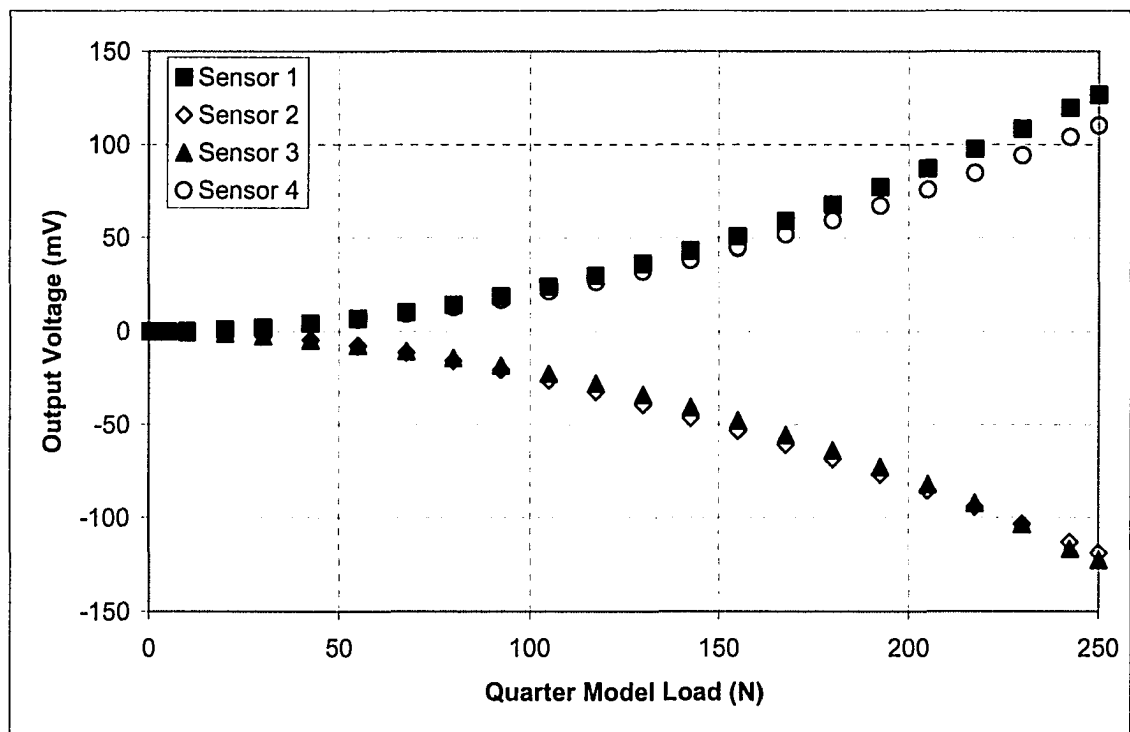


Figure 3.8. Simulated sensor outputs for the normal loading scenario.

Chapter 4 – Evaluation of Device Output Sets[†]

Through analysis of data transmitted from all four sensor pads, this chapter shows that it is possible to resolve three dimensional forces and moments occurring between the rod and the screw or hook. General equations using data from all four sensor pads are defined to convert the combination of signal patterns back into forces and moments. A manufacturing scheme for a prototype sensor is also described. Finally, the validity of these general equation forms is evaluated through analysis of this prototype's performance. The analysis of the prototype also serves as a means to verify the finite element analysis.

4.1 –Loading Scenario Descriptions

4.1.1 – Definition of Coordinate Systems

The forces and moments applied at any location can be fully defined in three dimensions by a combination of three forces and three moments acting on three separate, orthogonal axes. For the case of each hook or screw used in scoliosis correction surgery, the origin is defined at a point in the center of curvature of the hook notch, at the halfway point along the length of the hook or screw head. Axis one is defined as a direction parallel with the hook notch, generally collinear with the axes made by both the rod and the spinal column. Axis two is defined as a direction from the origin through the sidewall of hook or screw head, generally lateral to the spinal column and rod. Axis three, the previously defined “normal” direction, is aligned with the axis of the screw, generally in an anatomic anterior-posterior direction and orthogonal to axis one and two. Figure 4.1 shows these axes, along with their associated forces and moments, relative to a hook or screw head.

A second set of coordinate systems is defined relative to the strips, since output voltages have been calibrated for each pad in coordinate systems aligned with the strip surfaces. Each sensor pad is given a letter designation, A, B, C, and D according to the pattern shown in Figure 4.1. These four coordinate systems are located at the center of the membranes on their surfaces. Positive directions for these systems are out of the pad

[†] Portions of this chapter were presented at the 2005 ICMENS conference.

surface plane for the normal “N” directions and toward the outside of the hook body for the tangential “T” directions. The remaining axis for each pad is parallel with axis one (“1”) in the hook or screw coordinate system. These adjusted coordinate systems are shown in Figure 4.2.

4.1.2 – Description of Applied Loads

Using the coordinate systems defined in section 4.1.1 with the positive directions as indicated in Figures 4.1 and 4.2, the different signal patterns produced by each of the four sensor pads during application of loads to the rod can be predicted. This information is important for distinguishing the different load cases, and also for defining equations to quantify the magnitude of each of the global forces. Table 4.1 shows the general signal patterns that can be expected on each of the four (A,B,C,D) sensors for positive application of F_1 , F_2 , F_3 , M_1 , M_2 and M_3 . As specified in section 4.1.1, the signals will be presented in terms of the coordinate system of each sensor, and will be indicated by a positive or negative sign followed by the axis that the expected signal acts upon (1,T or N).

Table 4.1. Expected signal patterns during hook load application

Hook or Screw Force Direction	Sensor A	Sensor B	Sensor C	Sensor D
F_1	+1	+1	+1	+1
F_2	+N, -T	+N, -T	-N, +T	-N, +T
F_3	+N, +T	+N, +T	+N, +T	+N, +T
M_1	-T	-T	+T	+T
M_2	-N, -T	+N, +T	-N, -T	+N, +T
M_3	+N, -T	-N, +T	-N, +T	+N, -T

It can be seen that the six load directions each produce a distinct signal pattern. Negative values of the hook or screw force directions will produce similar signal patterns with the signs on the sensor data reversed. The load patterns shown should allow multiple loads to be detected through properly posed general equations.

4.2 – Resolving Loads from Input Voltages

The data in Table 4.1 can be used to create general equations that will allow hook and screw forces and moments to be resolved in a general loading scenario. Initially, pad equations similar to those presented in section 3.3.3 (18-20) will be used to convert voltage outputs to forces in the I, N and T directions. The force values for each sensor are then inputted into the new general equations. In order to differentiate values from each sensor, the letter designation of each sensor will be followed by a subscript indicating the applicable force direction. For example, forces on sensor A acting on the I, normal and tangential axes will be represented as A_I , A_N and A_T , respectively. Constants occurring in the equations will be designated k_n . These constants have been used in places where actual device calibration may be necessary to ensure accuracy of the equations.

The F_I load case involves shear loads applied evenly to each pad as the rod attempts to slide along the axis of the hook notch. The general equation is:

$$F_I = k_1 (A_I + B_I + C_I + D_I) \quad (21)$$

The F_2 load case involves a positive normal load and negative tangential load applied to the pads on one side of the notch, and a negative normal load and a positive tangential load applied to the pads on the other side of the notch. The general form of the equation is:

$$F_2 = \frac{A_N + B_N}{k_2} - \frac{C_N + D_N}{k_3} - \frac{A_T + B_T}{k_4} + \frac{C_T + D_T}{k_5} \quad (22)$$

The F_3 load case is the normal load case, and will be present to some extent for all other load application modes (due to the retaining bolt). This load applies positive normal and tangential loads to evenly to all four sensor pads.

$$F_3 = \frac{A_N + B_N + C_N + D_N}{k_6} + \frac{A_T + B_T + C_T + D_T}{k_7} \quad (23)$$

The M_I load case is a torsion load along the axis of the rod. This load applies shear loads along the tangential axis of all four sensor pads. These loads are relatively even in magnitude, but will vary in direction depending on where they are located in the hook or screw notch. The general equation is:

$$M_I = k_8 (C_T + D_T - A_T - B_T) \quad (24)$$

The M_2 load case is effectively the difference in F_3 (normal loading) values between sensor pads at either end of the hook notch (the two groups are A, C and B, D) divided by the distance between them. This can be represented by an equation in the form of:

$$M_2 = k_9 \left[\left(\frac{B_N + D_N}{k_{10}} + \frac{B_T + D_T}{k_{11}} \right) - \left(\frac{A_N + C_N}{k_{12}} + \frac{A_T + C_T}{k_{13}} \right) \right] \quad (25)$$

The M_3 load case is similar to the M_2 load case except it is representative of a difference between F_2 values at either end of the hook notch. As expected, this equation is similar to (25) and takes the form:

$$M_3 = k_{14} \left[\left(\frac{A_N}{k_{15}} - \frac{C_N}{k_{16}} - \frac{A_T}{k_{17}} + \frac{C_T}{k_{18}} \right) - \left(\frac{B_N}{k_{19}} - \frac{D_N}{k_{20}} - \frac{B_T}{k_{21}} + \frac{D_T}{k_{22}} \right) \right] \quad (26)$$

To prove the validity of these equations, a moment in the M_2 direction is considered. From Table 4.1, general values of forces are used ($A_N = -N$, $B_T = +T$, etc.). For simplicity in this example, all constants are set to unity ($k_n = 1$). Outputs for (21-26) for this application of loads are shown in Table 4.2.

Table 4.2. Calculated values for sensor output in a hypothetical M_2 load application scenario.

$F1$	$F2$	$F3$	$M1$	$M2$	$M3$
0	0	0	0	4N + 4T	0

These outputs show that application of a pure moment in the M_2 direction does not produce any false positives for loading in other directions. A similar trial can show that these equations are equally effective in the case of superimposed loading.

4.3 – Prototype Manufacturing

4.3.1 – Motivation

Finite element analysis has been used to calculate values for the constants in (21-26), and also has produced some alternate forms of (18-20) that have been adapted for variations in the sensor design. These values and equations have not been included here. Experience gained during the manufacturing and testing of a prototype piezoresistive sensor has shown that variability between the finite element results and the prototype's

performance may be significant. This variability implies that the finite element results alone may not be accurate enough to be used to create legitimate equations characterizing the outputs of the sensor system. Calibration of the manufactured sensors will need to be performed to characterize the system.

The software used for finite element simulation of MEMS and multiphysics devices is currently developing and becoming very comprehensive. These advances challenge the conventional methodology of the production of such devices, where mechanical performance may remain largely undetermined until a prototype is built. The use of such software is advantageous in this application, as building prototypes at each design revision of the scoliosis sensor would have been extremely complicated and expensive. However, difficulties may also arise if device characterization is done exclusively with FEA. It is difficult to know how well the FEA simulation reflects actual geometry until a prototype is built, and variations and imperfections in the device created by the manufacturing process will certainly affect device performance to some degree.

Specific deviations that are produced in the manufacturing process of this device that are not easily incorporated into finite element models may include geometrical and electrical anomalies. Geometrical anomalies include curvature on the etched side of the membrane cavity, variation in the overall thickness of the membrane, edges and corners that become rounded. Electrical anomalies include the presence of significant leakage current at elevated temperatures, resistivity per unit length that depends on the local bias across the isolation diode, and capacitive artifacts in the piezoresistors. By evaluating the performance of a prototype piezoresistive sensor, it is possible to determine how accurately a piezoresistive MEMS device can be characterized using an ideal finite element model.

4.3.2 – Prototype Sensor Description

The sensor design selected for characterization is not identical to the contact force sensors for use in scoliosis correction surgery described previously. This is due to a problem with the manufacturing process rendering the described scoliosis sensors inoperable. Fortunately, other devices utilizing an alternate design from the same batch were still functional, so they were characterized in place of the scoliosis devices. The

characterized devices are similar in structure to a silicon pressure sensor [39], with thicker membranes and altered resistor patterns. This sensor design is shown in Figure 4.3, and the electrical connectivity is shown in Figure 4.4. The characterized devices use four linear piezoresistors in a Wheatstone bridge configuration rather than the four-terminal gauges that the scoliosis sensors utilize. This is the most significant difference between the two devices, and may create inaccuracies due to the differing electrical connections and sensing schemes used in the two types of devices. Despite this, important similarities exist between the two devices that allow this prototype to serve as an effective characterization model. Both devices utilize doped piezoresistors and membranes; having similar features is an important factor in the evaluation of the finite element analysis. Additionally, both share an atypical load application method for piezoresistive sensors; forces are distributed over a small section of the membrane instead of having a pressure distributed over the entire surface.

A custom procedure was developed for manufacturing these sensors at the University of Alberta's Nanofab facility. A simplified schematic of the manufacturing procedure used is shown in Figure 4.5. The sensors are built on 500 μm n-type (100) silicon substrates that are initially cleaned and marked for alignment. All photolithography masks used in this process were made at the Nanofab facility. The piezoresistors are specified to be 20 μm x 200 μm p-type regions that are specified by opening "diffusion windows" by exposing, developing and etching portions of a photoresist layer. Doping is then performed through these windows with a boron diffusion and thermal drive-in process (1 μm depth). This selective doping procedure forms junction-isolated resistors. For maximum sensitivity, the long axes of the resistors are aligned with the $\langle 110 \rangle$ direction on the (100) plane. A masking layer is applied, followed by more lithography to open windows to allow the metal to contact the piezoresistors at specific places. An aluminum layer is sputtered on and then patterned to provide electrical connectivity. Square 1mm x 1mm membranes are then created by making a cavity on the backside of the substrate with a DRIE etch. This process produces nearly vertical cavity walls and is timed for a depth of 435 μm , making the membranes approximately 65 μm thick. The silicon substrate can then be diced to separate the individual sensors.

4.4 – Prototype Performance Evaluation

4.4.1 – Comparison Methodology

In order to determine the accuracy of a finite element characterization, the following procedure is performed: An ideal FEA model will be produced and the results of this analysis will be compared to a manufactured device prototype. A second FEA model will then be produced based on dimensions from the actual model and the degree of congruency between all three data sets will be compared.

The test procedure for these sensors involves applying a 5V source voltage as specified in Figures 4.3 and 4.4 and applying a distributed force to a small area in the center of the membrane. Output voltages can then be collected from the free electrodes on the Wheatstone bridge circuit as the applied force is varied. Although this load application method differs from typical pressure loads experienced by this type of membrane sensor, the maximum stresses will still occur at the midpoint of the diaphragm edges. In a more practical sense, a point load at the center of a membrane will produce stresses approximately double those produced if the same load was distributed over its entire surface. See section 2.4 for an extended explanation. Further support of the use of a membrane sensor for contact force measurement is found in the simulation output data. Pressure and force loading both produce results which are highly linear, and both are found to follow theoretical predictions closely in this analysis.

4.4.2 – Finite Element Characterization

The idealized finite element model is evaluated first. The dimensions of this model are taken from those specified in the manufacturing procedure, and a mesh size of 10 μ m was found to produce accurate results. The edges of the model are assumed to be perfectly square, which is an approximation that is particularly inaccurate on the underside of the membrane and in the transition regions between the doped and un-doped silicon. Models tested are constrained on the lower surface of the substrate. The simulated load on the center of the membrane was provided by a distributed force load applied on a square area (20 μ m x 20 μ m) on the top surface of the sensor. Electrical boundary conditions and loads were applied directly to the contact locations of the piezoresistors as aluminum contacts were omitted for simplicity. The multiphysics analysis used allows voltage

outputs to be obtained directly as the simulated load is applied. Data set A in Figure 4.6 shows the output produced for the ideal model with a 65 μ m membrane.

The finite element model used provides a very robust solution for calculating properties of the sensors. Changes to the model can be made very easily, allowing for characterization of several sensor properties. Figure 4.7 shows how ideal model sensitivity varies with membrane thickness and Figure 4.8 shows how moving the location of the applied force away from the center (toward a corner of the membrane) changes the sensitivity. Finite element analysis was also used to simulate the performance of the sensors that were actually tested. After collecting specific geometric information from the sensors, replica models closely resembling the actual sensors were built. Sensitivity of these replica sensors is shown as data sets B2 and C2 in Figure 4.6.

4.4.3 – Experimental Characterization

The manufacturing and testing of the devices was performed using custom processes at the University of Alberta Nanofab. The sensors were not packaged before testing, so a probe station was modified to determine the sensitivity of two prototypes. A schematic and photo of the modification are shown in Figures 4.9 and 4.10. A force load is applied by pressing downward on the center of the membranes with a probe. This force is quantified by measuring the force change detected by a balance on which the whole sensor is resting. Electrical output was collected by connecting the bridge circuit to four other probes on the probe station. Signal outputs from the experimental trials are shown in Figure 4.6 as data sets B1 and C1. These data sets have had offset voltages caused by bridge resistor imbalances removed. This was done to fit them on the same plot as the FEA results and did not affect sensitivity calculation.

In order to build finite element replicas of the actual sensors tested, exact measurements of the manufactured sensors need to be made. Overall thickness of the wafer section was measured with an anvil micrometer, and a cross-section of the cavity was measured using an optical profilometer. Cross-sectional profiles of each sensor are shown in Figures 4.11 and 4.12. The undersides of the membranes are fit to the equations shown in the figures in order to build the specified profiles into the replica finite element models. Typical boron diffusion profiles [40] are also added to the FE

models to make the doped/un-doped transition region resemble the actual models more closely. Measurements on the upper surface of the sensors were also taken to ensure that the geometry of the piezoresistive regions corresponded to the dimensions used in the finite element analysis.

4.4.4 – Prototype Characterization Results

The finite element model was built without incorporating any manufacturing abnormalities. This “ideal” sensor has a simulated sensitivity of 0.3843mV/mN with 5V excitation voltage. The output from this model also has excellent linearity. Converged output data was obtained quickly with this model, which allowed the effects of geometric variations on performance to be quickly analyzed. Empirical equations for sensitivity when varying membrane thickness (Figure 4.7) can efficiently be produced with the ideal model. These results were found to correspond to performance curves for pressure sensors found in literature [39]. Sensitivity when varying the distance from membrane center to edge is also easily performed with this model. Results and the empirical equation fit are shown in Figure 4.8. These results are consistent with those found theoretically [32], with maximum sensitivity found when the force distribution is applied to the center of the membrane and minimum sensitivity found when the force distribution approaches the corner of the square membrane.

Comparing the sensitivity of the ideal FE sensor to the prototype trials shows that the prototypes are much less sensitive than the ideal sensor with sensitivities of 0.2075mV/mN and 0.0291mV/mN for prototype 1 and 2, respectively with 5V of excitation. Much of the sensitivity variation between the sensors and the ideal model, as well as variation between each of the prototypes, is due to variation in the thickness of the membranes. This variation was created in the manufacturing process and is a function of etch time and location of the sensor on the substrate. When the ideal models are altered to have a membrane thickness equivalent to the average membrane thicknesses of prototype 1 and 2 (31 μ m and 79 μ m, respectively) the ideal sensitivities become 1.789mV/mN and 0.2554mV/mN. These variations to the ideal model do not produce results that are individually closer to the performance of the actual prototypes, but by examining both sets of data it can be seen that both the modified ideal models and

the prototypes have a sensitivity ratio for thin membrane sensor (prototype 1) to thick membrane sensor (prototype 2) of approximately 7. This shows that while the ideal simulation may not produce results that are identical to the manufactured prototypes, general performance trends obtained in the ideal simulations are accurate.

To better simulate geometric effects on sensor performance, replica models based on the actual dimensions of the prototypes were produced. Sensitivity from these replicas showed better correlation with the actual prototypes; simulated sensitivities were 0.8909mV/mN and 0.2101mV/mN for simulated models 1 and 2, respectively. Despite improvements in sensitivity errors over the ideal models, replica model sensitivities still exceed the prototype trials by a factor of 4.3 for prototype 1 and a factor of 7.2 for prototype 2. Replica models also do not appear to follow the same trend of sensitivity to thickness that the ideal models and the prototypes follow; the sensitivity ratio of replica 1 to replica 2 is 4.2 rather than approximately 7. This trend is likely in part due to the different shape of the membranes for sensors of different thicknesses. As Figures 4.11 and 4.12 illustrate, the underside of the membrane of replica 2 is more flat than replica 1. Less curvature on the underside of the membrane indicates that replica 2 more closely resembles the ideal model (with the flat underside). This is supported in the performance of the model sensors when comparing the sensitivity of ideal models to replica models. Replica 1, which has more curvature, has a sensitivity of about 50% of the ideal model, while replica 2, with less curvature, has a sensitivity of 82% of the ideal model.

There are several possible explanations for the sensitivity being lower on the prototypes. The most obvious explanation is that the probe applying the normal force was not centered on the membrane. As depicted in Figure 4.8, ideal case sensitivity will be reduced by 50% when the force is applied approximately 300 μ m from center and reduced by 90% when the force is applied approximately 440 μ m from center. Deviations from membrane center are possible. The probe was manually positioned over what was assumed to be the center of the membrane, but because the probe was viewed from above the point of contact was hidden behind a 90° bend above the probe tip. Other possible explanations for reduced sensitivity include diode effects at the metal-piezoresistor interface creating leakage current, decreased $\Delta R/R$ due to conductor damage or

inefficiency, or signal loss due to imperfect contact between the electrical probe tips and the contact pads on the actual circuits.

This comparison of finite element results with actual prototypes of a MEMS force sensor is useful when determining the extent of characterization and design that can be done with FEA. This has shown that geometric and electrical variability created in the manufacturing procedure prevents exact characterization of the prototype or scoliosis sensors. Despite this inability, it is shown that general trends in performance are easily characterized with FEA, which can be very useful in all but the final stages of the design process and can limit the number of design modifications that need to be made after the manufacturing stage of product development has begun.

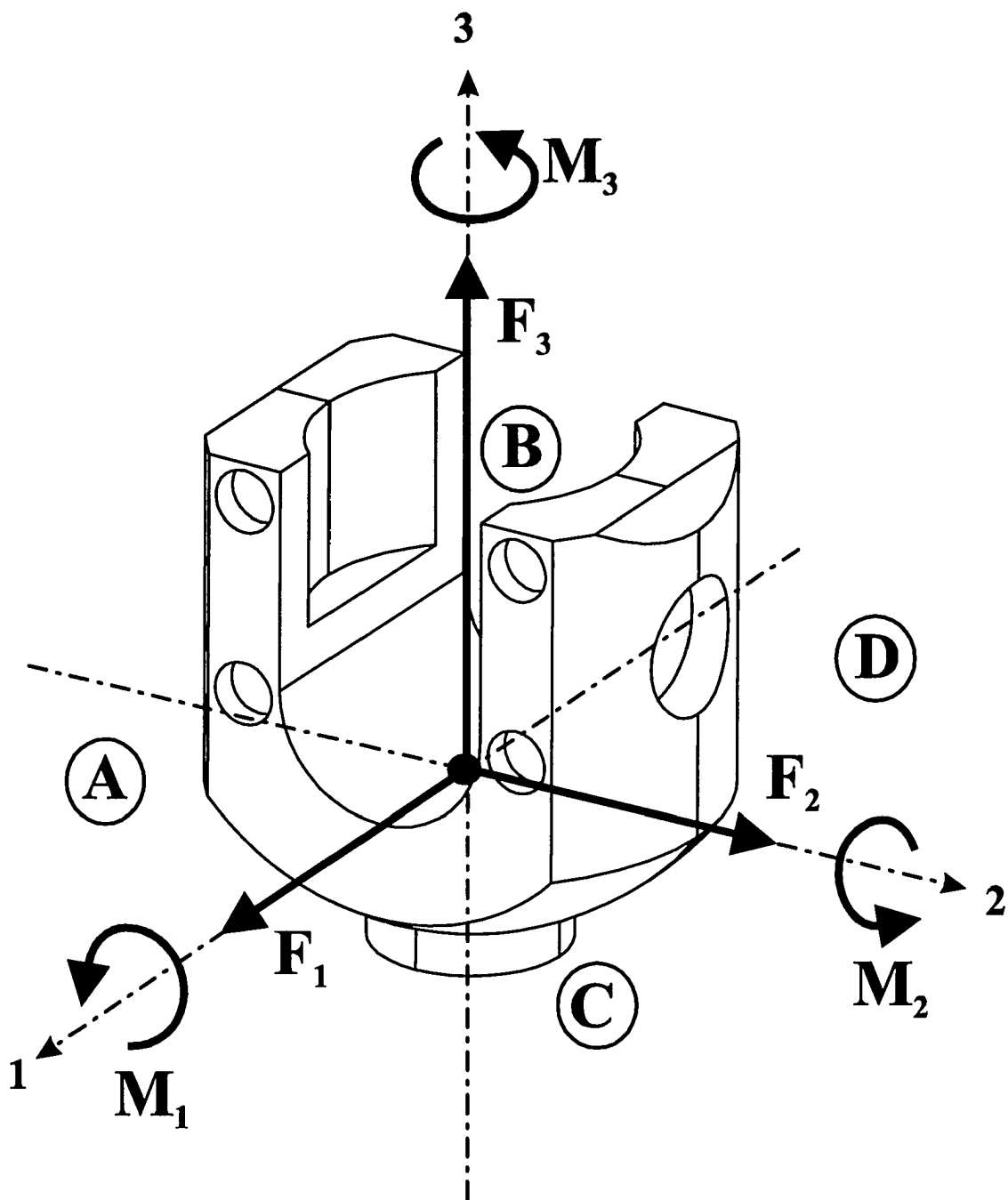


Figure 4.1. Coordinate system for each hook or screw head. Letters indicate relative locations of sensor pads on the device.

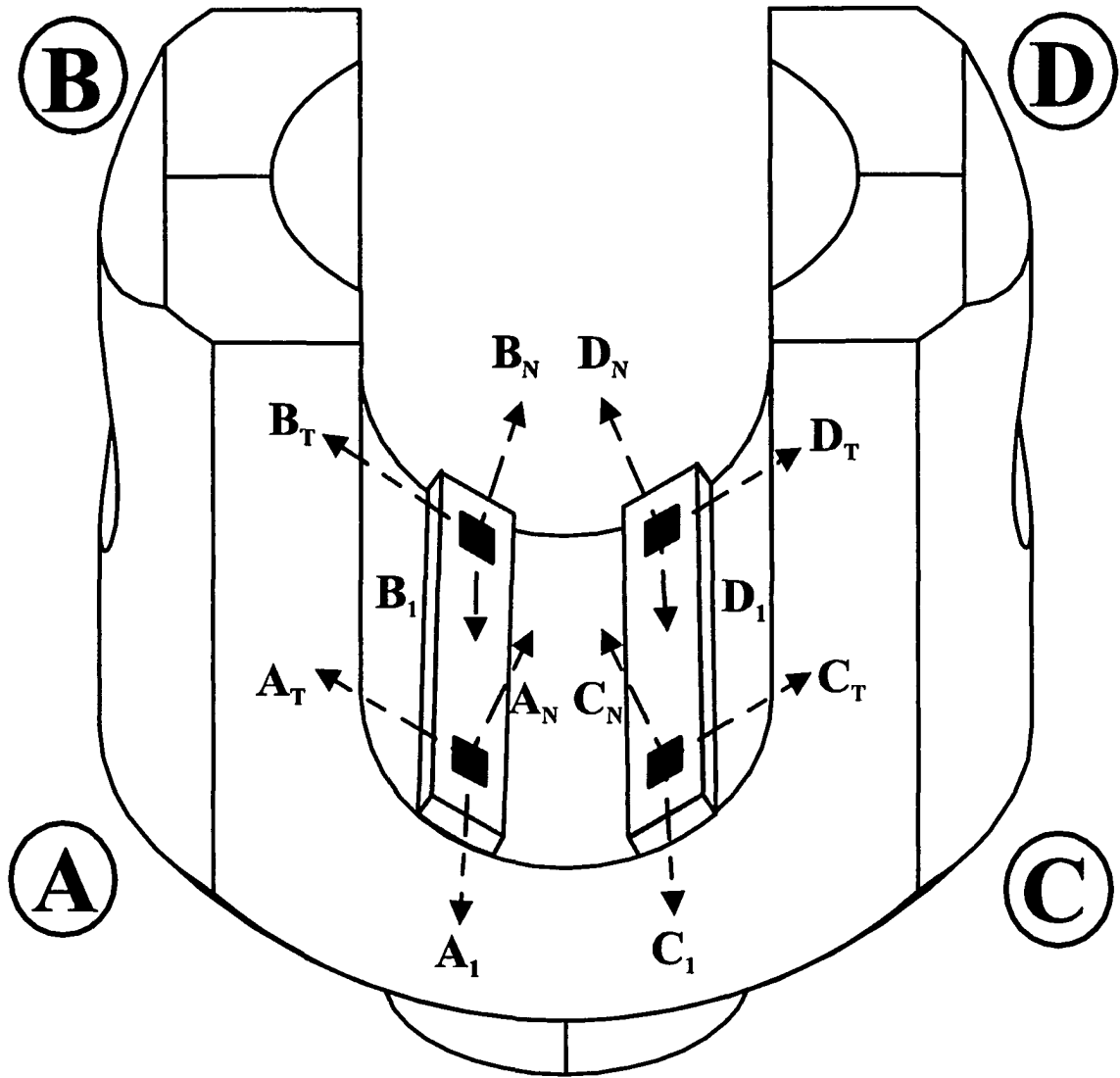
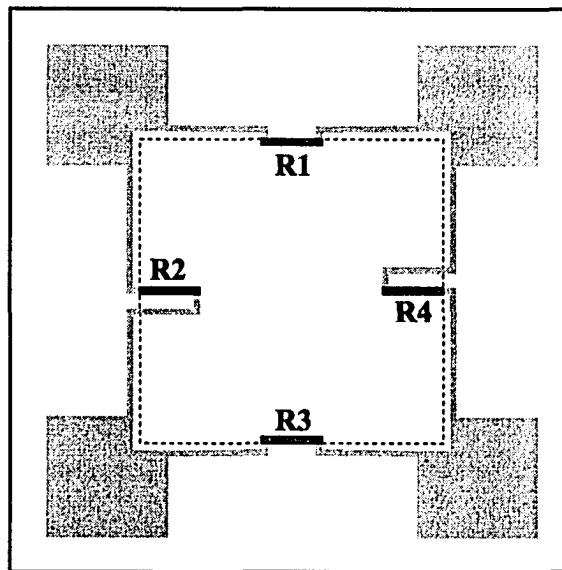


Figure 4.2. Coordinate systems for each pad.






-  - Aluminum Conductor
-  - Membrane Cutout
-  - Piezoresistive Material

Figure 4.3. Schematic of the manufactured device.

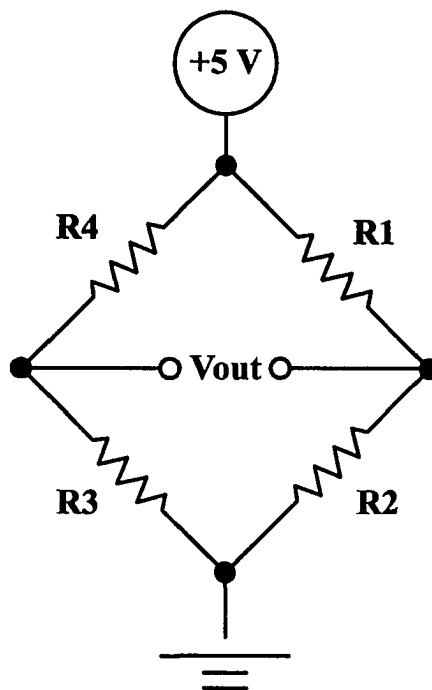


Figure 4.4. Electrical connectivity of the manufactured device.

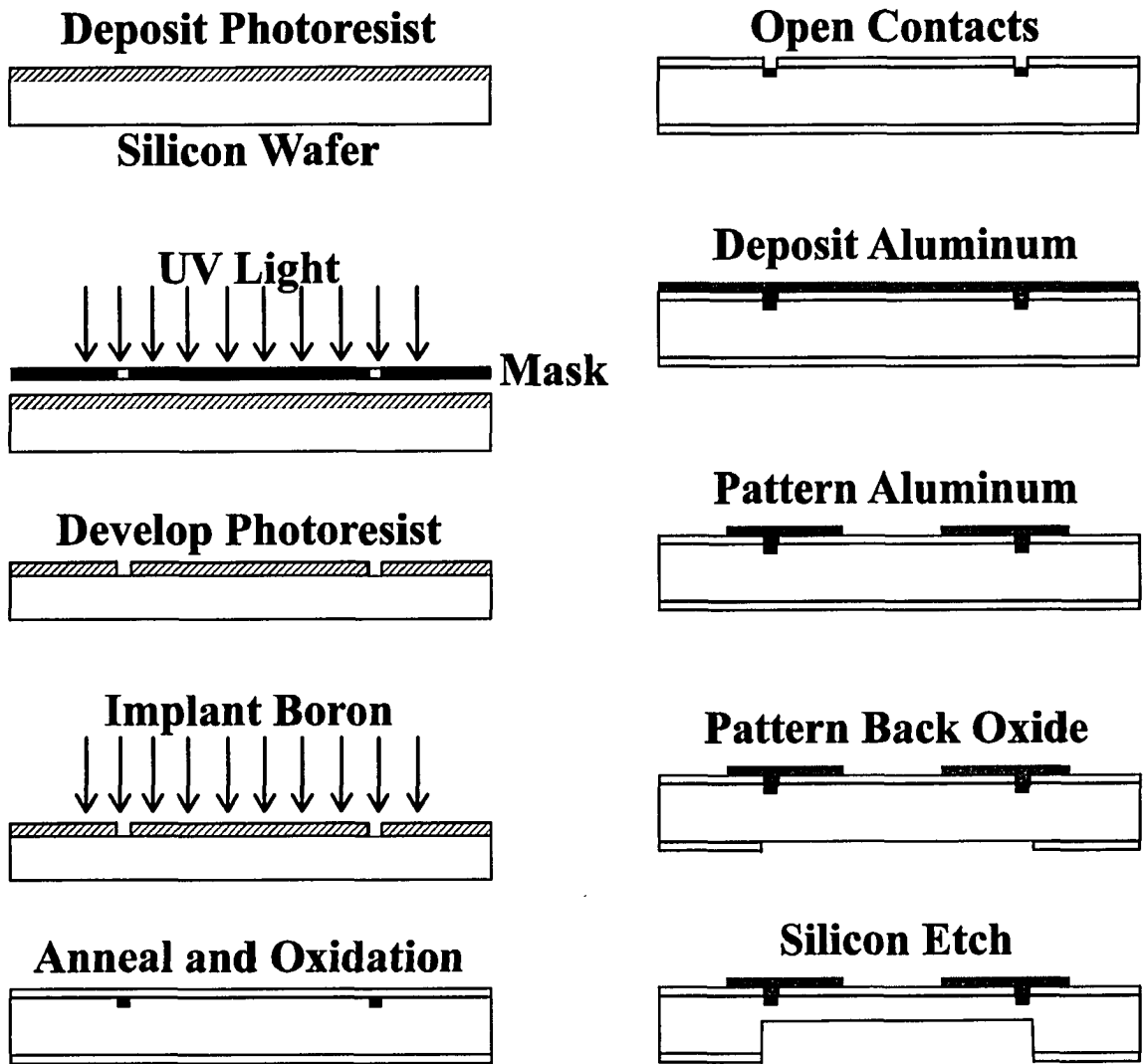


Figure 4.5. Piezoresistive sensor manufacturing scheme. (Modified from [41].)

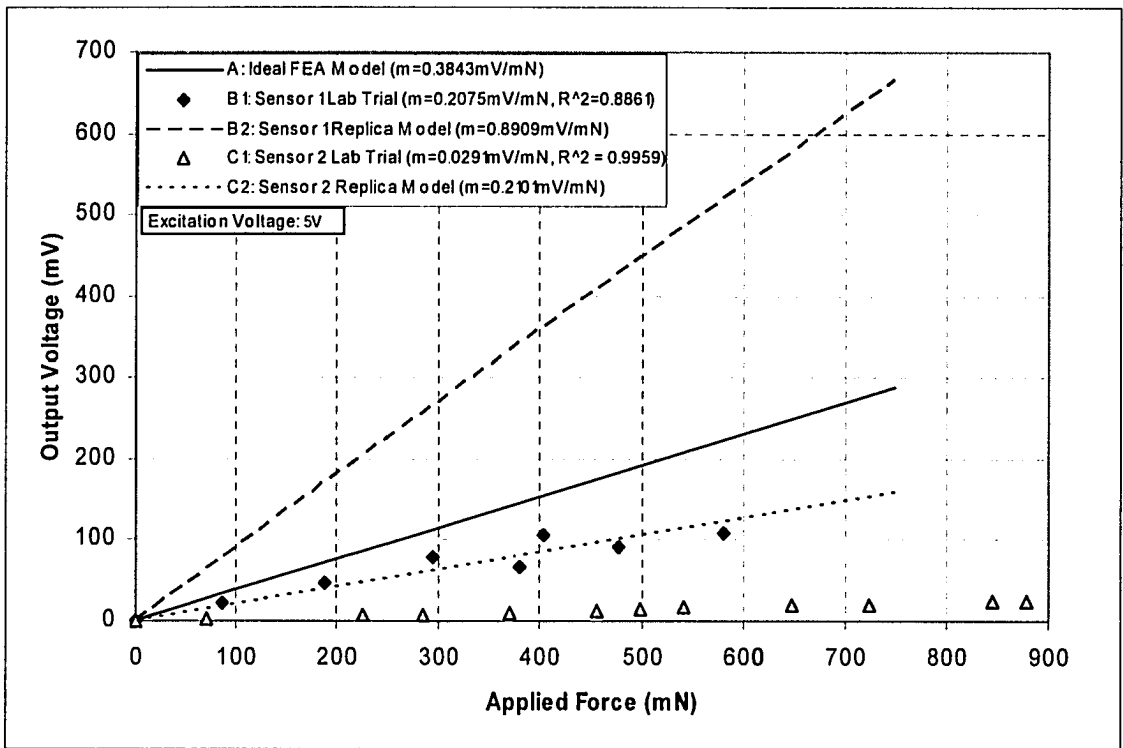


Figure 4.6. Data sets from sensor testing and simulation.

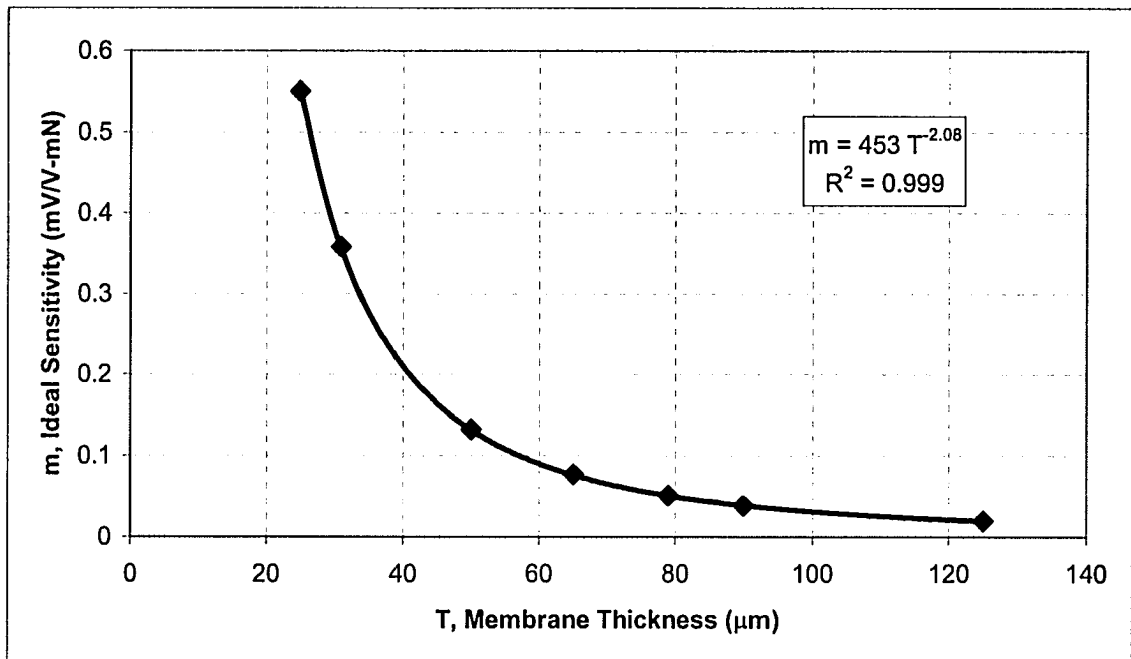


Figure 4.7. Sensitivity variation as ideal membrane thickness is adjusted.

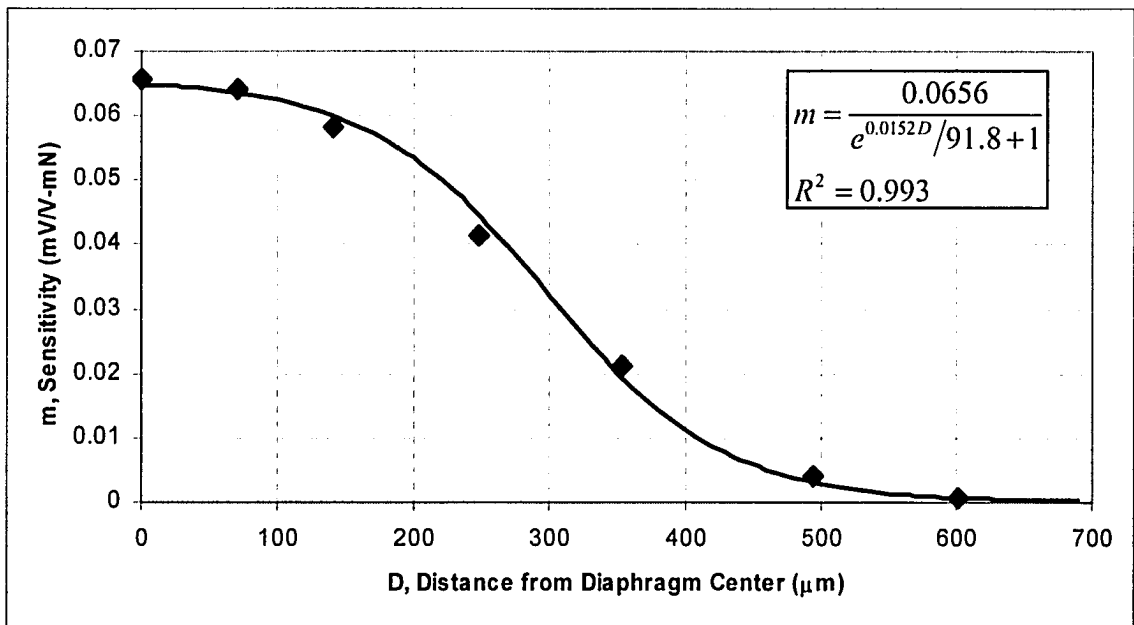


Figure 4.8. Sensitivity variation as the force application site is moved away from diaphragm center.

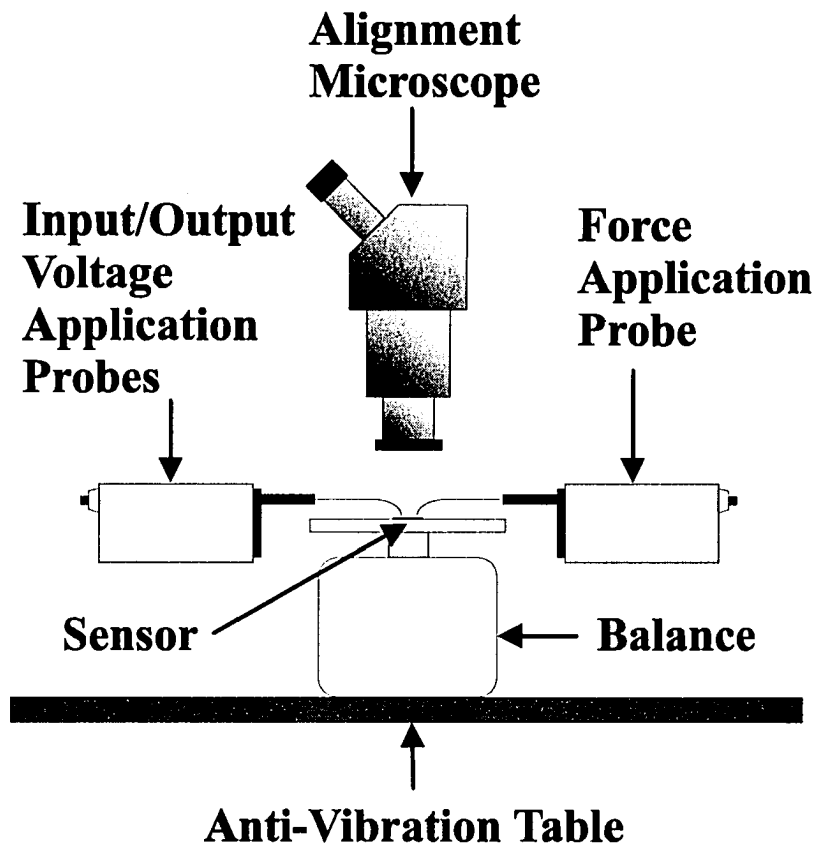


Figure 4.9. Schematic of the sensor characterizing apparatus.

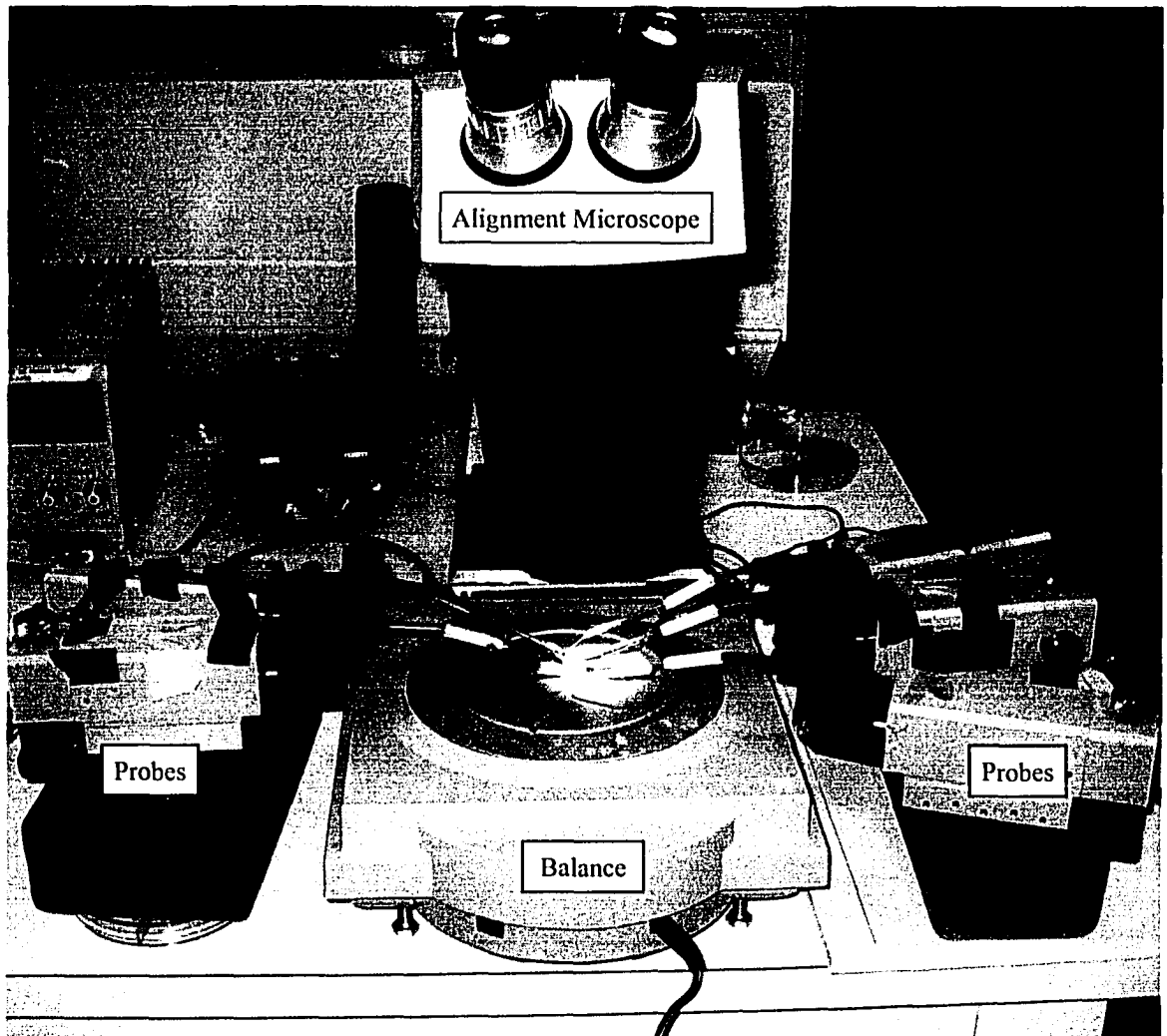


Figure 4.10. Photo of the sensor characterizing apparatus.

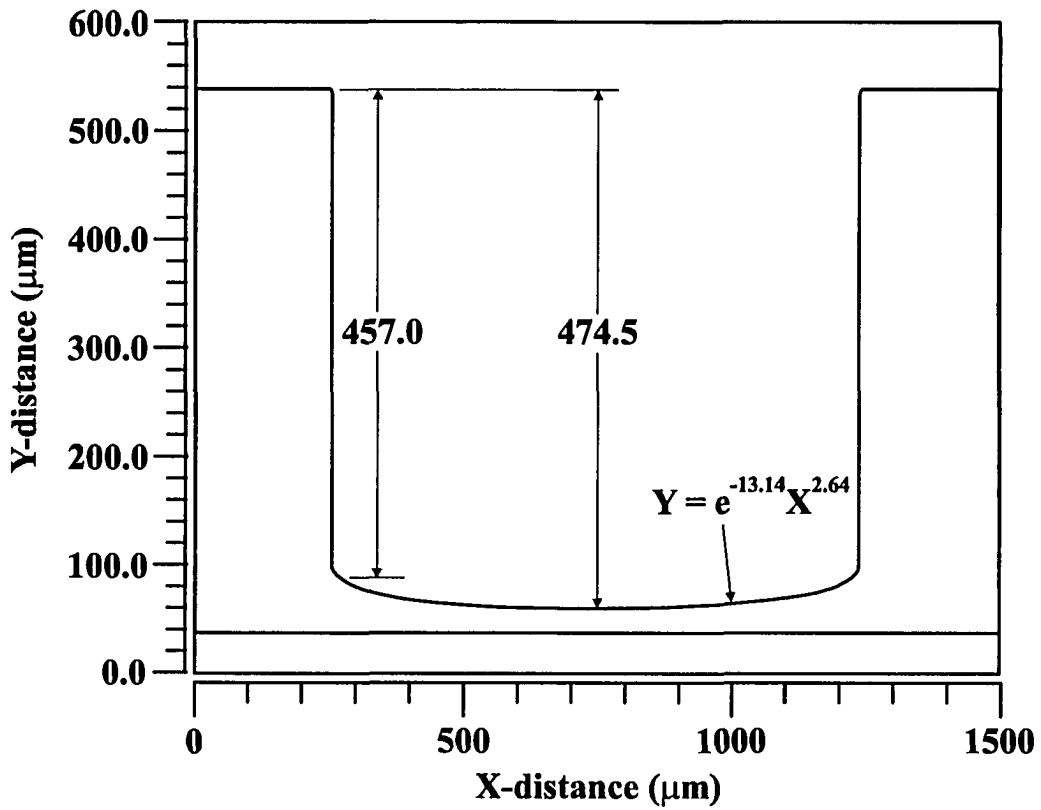


Figure 4.11. Cross-sectional profile of experimental sensor 1.

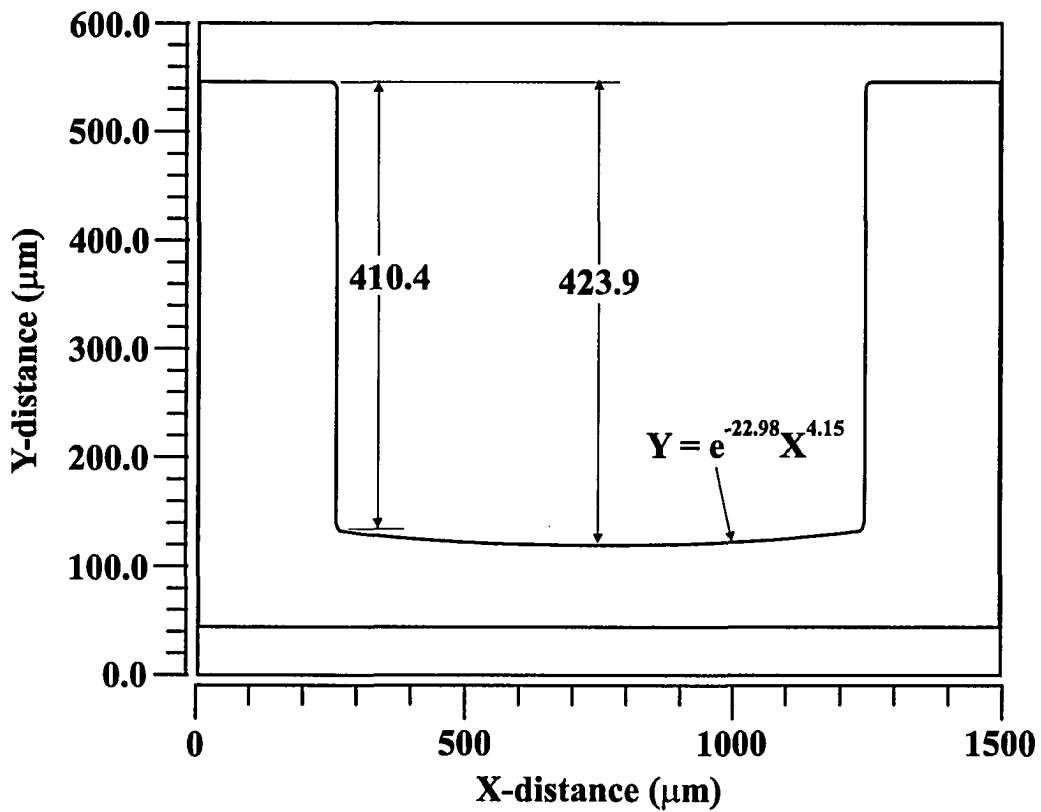


Figure 4.12. Cross-sectional profile of experimental sensor 2.

Chapter 5 – Conclusions

The current state of this research project is described. The major objectives are reiterated, the steps already taken to reach these objectives are listed, and the remaining steps that are necessary to conclude this project are detailed. Future uses for this sensor system as the industry develops are also discussed.

5.1 – Achieved Objectives

The primary goal of this research is to design a wireless sensor to measure the loads applied and distributed along the spine during scoliosis correction surgery. The system that has been designed is effectively an instrumentation system for the hooks and screws used to fix the corrective rod to the spine. This design includes three major components affixed to each hook or screw: A battery to provide system power; a wireless transmitter to send data to an external device where it can be displayed and stored; and two sensor strips to detect the loads between the hooks/screws and the rod. The sensor strips are the major focus of this portion of the research. Using FEA and conventional design techniques, strips using embedded sensors have been developed that are able to detect forces and moments in three dimensions.

Due to size and performance constraints, it was decided that the strips should be piezoresistive MEMS devices. MEMS devices have several advantages, including small size, low relative cost, low power consumption and compatibility with wireless technology. In order to detect forces and moments in all required directions, each strip has two sensing pads built-in, located near each end. These sensing pads are sensitive to forces normal and tangential to their surfaces. Each pad and consists of an etched silicon membrane with four piezoresistive four-terminal sensors near the center of each membrane edge. The four-terminal sensors allow the forces and moments applied between the rod and hook/screw to be converted to voltage outputs, which can be sent to an external device for analysis, display and storage.

In order to establish that the design parameters of this sensor are valid, FEA has been used extensively to prove this sensor system. A finite element model of the hook/screw head and rod was used very early in the sensor development. It was used to

find the stress distribution in the hook and screw body during the application of various forces and moments. Stress distributions were examined to find locations where sensors could be used to measure the forces and moments in this application. After the sensing scheme with sensor strips within the notch was developed, FEA was used to determine the location and orientation of the strip within the notch, as well as the location of the sensor pads on the strips. In terms of the sensor strips themselves, FEA trials were performed to determine appropriate membrane thicknesses, as well as sizes and orientations of piezoresistors. FEA was also used to model the performance of the sensor and to verify that the proposed design is capable of measuring forces and moments in three dimensions.

To further evaluate the viability of the designed sensor, a device was manufactured using a typical protocol for a piezoresistive membrane sensor. This device was not identical to the strips used in the proposed device, but it possessed many of the same features. Evaluation of the manufactured device in the lab through application of a contact load allowed comparison with finite element results. This comparison determined that the performance of the manufactured sensor will not be identical to the finite element model, but it will obey the same general trends in performance.

5.2 – Continued Development

Although a viable design and manufacturing scheme are presented, this project is by no means concluded. Several steps remain before a prototype hook or screw that can be tested surgically is completed. First, sensor strips need to be manufactured. These strips then must be physically characterized to determine if they have been built within required tolerances and perform as predicted. A method for dicing the (very small) strips must also be developed. The diced strips then need to be attached to the hook and connected to the transmission and battery modules. This poses a significant challenge, as the geometry of the hook notch is complicated and the system needs to be both rugged (to survive sterilization and surgery) and biocompatible. Once the hooks and screws are instrumented appropriately, they need to be calibrated in the laboratory with known loads to fully determine the calibration equations.

With the calibration equations and instrumented sensors, the wireless network system will need to be built and tested for use in an operating room environment. Significantly more electrical noise exists in a surgical setting than in a laboratory, so the design of the wireless components will have to be adequately robust. In addition, during surgery each sensor will be transmitting 16 voltages that will need to be converted to forces and moments. In a situation where every fixation screw and hook is instrumented, this could equate to over 100 signals transmitting simultaneously, which could overwhelm the receiving device and associated software. In order to make this large amount of information useful in the operating room, software must be developed to display the loads applied to the spine in a clear and easily understandable manner.

As other components are developed, the functionality of this sensor system will continue to grow. If the force loads collected during surgery are combined with displacement data collected with a spinal telemetry system, a large amount of spinal stiffness information could be collected. This information could be used to improve many of the numerical spinal models currently in use. Spinal stiffness is also essential information for pre-surgical planning models. When this sensor system has proven itself in the surgical setting, and a permanent or rechargeable power supply can be used, it may be possible to leave sensors in the body permanently. A permanent system would be useful as a means to detect post-operative equipment failure, and also to monitor the healing process.

5.3 – Concluding Remarks

Despite the relative regularity of scoliosis correction surgery, there is not a significant amount of data available which quantifies the loads applied. Part of the lack of information is due to the complexity of the orthopedic instrumentation and corrective procedure, both of which make it difficult to measure the loads in a conventional manner. Building a system that is able to extract comprehensive information from the spine during surgical correction is a challenging and important engineering problem. The solution presented, when fully completed, has the potential to improve the safety of the procedure for patients, increase the quality of correction offered by the surgery, aide in the

collection of comprehensive information about the mechanical properties of the scoliotic spine and to use this information to create a model for pre-surgical planning.

Extensive FEA use and limited prototype testing have been used to develop a design that is viable (at least from this perspective) for measuring forces and moments applied during scoliosis surgery. This integration of MEMS with biomedical engineering has shown itself to be a feasible way to improve surgical protocols and operative success rates. Additionally, the design of this sensor system is general enough to enable its use in other applications, biomedical or otherwise, where wireless force detection is desired. Significant challenges and obstacles must still be overcome before this sensor will see large scale use, but this project shows what is possible in the future of surgery and sensor systems.

Bibliography

- [1] "Scoliosis Facts," Scoliosis Association Inc., 1993.
- [2] J. E. Lonstein, "The prediction of curve progression," *Journal of Bone & Joint Surgery*, vol. 66, pp. 1061-1071, 1979.
- [3] V. J. Raso, E. Lou, D. L. Hill, J. K. Mahood, M. J. Moreau, and N. G. Durdle, "Trunk distortion in adolescent idiopathic scoliosis," *Journal of Pediatric Orthopaedics*, vol. 3, pp. 222-226, 1998.
- [4] P. R. Harrington, "Treatment of scoliosis, correction and internal fixation by spine instrumentation," *Journal of Bone & Joint Surgery*, vol. 44A, pp. 591-610, 1962.
- [5] Y. Contrel, J. Dubousset, and M. Guillanet, "New universal instrumentation in spinal surgery," *Clinical Orthopaedics and Related Research*, vol. Feb;227, pp. 10-23, 1988.
- [6] H. K. Dunn, A. U. Daniels, and G. G. McBride, "Intraoperative force measurements during correction of scoliosis," *Spine*, vol. 7, pp. 448-455, 1982.
- [7] G. Elfstrom and A. Nachemsom, "Telemetry recordings in the Harrington distraction rod: A method for increasing the safety in the operative treatment of scoliosis patients," *Clinical Orthopaedics and Related Research*, vol. 93, pp. 158-172, 1973.
- [8] A. Rohlmann, F. Graichen, U. Weber, and G. Bergmann, "Monitoring in vivo implant loads with a telemeterized internal spinal fixation device," *Spine*, vol. 25, pp. 2981-2986, 2000.
- [9] K. K. Duke, "The Design of Instrumentation for Force Measurement During Scoliosis Surgery," *M.Sc. Thesis in Mechanical Engineering*. Edmonton: University of Alberta, 2001, pp. 114.
- [10] K. K. Duke, K. R. Fyfe, M. J. Moreau, J. K. Mahood, V. J. Raso, and D. L. Hill, "Computer modelling of hooks for use as intra-operative force sensors," in *Research into Spinal Deformities 3, Series Studies in Health Technology and Informatics*, vol. 88, A. Tanguay and B. Peuchot, Eds. Oxford: IOS Press, 2002, pp. 350-355.
- [11] K. K. Duke, D. L. Hill, M. J. Moreau, J. K. Mahood, V. J. Raso, and D. R. Budney, "Force measurement of the "derotation maneuver"," in *Research into*

- Spinal Deformities 2, Series Studies in Health Technology and Informatics*, vol. 59, I. A. F. Stokes, Ed. Oxford: IOS Press, 1998, pp. 109-112.
- [12] E. Lou, D. L. Hill, V. J. Raso, M. J. Moreau, and J. K. Mahood, "Instrumented rod rotator system for spinal surgery," *Medical & Biological Engineering & Computing.*, vol. 40, pp. 376-379, 2002.
- [13] A. v. Ooy and C. W. Geukers, "Results of CD operation in idiopathic scoliosis," *Acta Orthopaedica Belgica*, vol. 58 suppl. 1, pp. 129-133, 1992.
- [14] K. J. Guidera, J. Hooten, W. Weatherly, M. Highhouse, A. Castellivi, J. A. Ogden, L. Pugh, and S. Cook, "Cotrel-Dubousset instrumentation, results in 52 patients," *Spine*, vol. 18, pp. 427-431, 1993.
- [15] M. Rittmeister, K. Leyendecker, A. Kurth, and E. Schmitt, "Cauda equina compression due to a laminar hook: A late complication of posterior instrumentation in scoliosis surgery," *European Spine Journal*, vol. 8, pp. 417-420, 1999.
- [16] H. D. Been, C. J. Kalkman, H. S. Traast, and B. W. O. d. Visser, "Neurologic injury after insertion of laminar hooks during Cotrel-Dubousset instrumentation," *Spine*, vol. 19, pp. 1402-1405, 1994.
- [17] N. Najafi and A. Ludomirsky, "Initial animal studies of a wireless, batteryless, MEMS implant for cardiovascular applications," *Biomedical Microdevices*, vol. 6, pp. 61-65, 2004.
- [18] T. B. Tang, E. A. Johannessen, L. Wang, A. Astaras, M. Ahmadian, A. F. Murray, J. M. Cooper, S. P. Beaumont, B. W. Flynn, and D. R. S. Cumming, "Toward a miniature wireless integrated multisensor microsystem for industrial and biomedical applications," *IEEE Sensors Journal*, vol. 2, pp. 628-635, 2002.
- [19] G. Lin, K. S. J. Pister, and K. P. Roos, "Surface micromachined polysilicon heart cell force transducer," *Journal of Microelectromechanical Systems*, vol. 9, pp. 9-16, 2000.
- [20] J. Dargahi, M. Parameswaran, and S. Payandeh, "A micromachined piezoelectric tactile sensor for an endoscopic grasper - theory, fabrication and experiments," *Journal of Microelectromechanical Systems*, vol. 9, pp. 329-335, 2000.

- [21] B. J. Kane, M. R. Kutkosky, and G. T. A. Kovacs, "A traction stress sensor array for use in high-resolution robotic tactile imaging," *Journal of Microelectromechanical Systems*, vol. 9, pp. 425-433, 2000.
- [22] L. L. Chu, L. Que, and Y. B. Gianchandani, "Measurements of material properties using differential capacitive strain sensors," *Journal of Microelectromechanical Systems*, vol. 11, pp. 489-498, 2002.
- [23] J. McEntee, "Properties of silicon (electronic version)," Retrieved January 25, 2004.
- [24] K. Peterson, "Silicon as a mechanical material," *Proceedings of the IEEE*, vol. 5, pp. 420-457, 1982.
- [25] M. C. Hseih, Y. K. Fang, M.-S. Ju, G.-S. Chen, J.-J. ho, C. H. Yang, P. M. Wu, and T. Y.-F. Chen, "A contact-type piezoresistive micro-shear stress sensor for above-knee prosthesis application," *Journal of Microelectromechanical Systems*, vol. 10, pp. 121-127, 2001.
- [26] A. Sutor, R. Lerch, H.-P. Hoho, and M. Gavesi, "New CMOS-compatible mechanical shear stress sensor," *IEEE Sensors Journal*, vol. 1, pp. 345-351, 2001.
- [27] T. R. Chandrupatla and A. D. Belegundu, *Introduction to Finite Elements in Engineering*. Toronto: Prentice Hall, 2002.
- [28] M.-H. Bao, "Handbook of sensors and actuators, Volume 8: Micromechanical Transducers," Elsevier Science, 2000, pp. 199-239.
- [29] "Section 7.5," in *Ansys 8.1 Help Documentation*, 2004.
- [30] J. E. Shigley, C. M. Mischke, and R. G. Budynas, "Contact Theory," in *Mechanical Engineering Design*, 7 ed. Toronto: McGraw Hill, 2004, pp. 161-166.
- [31] J. O. Smith and C. K. Liu, "Stresses due to tangential and normal loads on an elastic solid with application to some contact stress problems," *Journal of Applied Mechanics*, vol. 71, pp. 157-166, 1963.
- [32] S. Timoshenko and S. Woinowsky-Krieger, *Theory of Plates and Shells*. Toronto: McGraw-Hill, 1959.
- [33] H. M. Westergaard and W. A. Slater, "Moments and stresses in slabs," *Proceedings of the American Concrete Institute*, vol. 17, pp. 415-538, 1921.

- [34] A. P. Boresi, R. J. Schmidt, and O. M. Sidebottom, *Advanced Mechanics of Materials*, 5 ed. New York: John Wiley & Sons, 1993.
- [35] W. G. Pfann and R. N. Thurston, "Semiconductor stress transducers utilizing the transverse and shear piezoresistance effects," *Journal of Applied Physics*, vol. 32, pp. 2008-2019, 1961.
- [36] M.-H. Bao, W.-J. Qi, and Y. Wang, "Geometric design rules of four-terminal gauge for pressure sensors," *Sensors and Actuators*, vol. 18, pp. 149-156, 1989.
- [37] Y. Kanda, "Optimum design considerations for silicon pressure sensors using a four-terminal gauge," *Sensors and Actuators*, vol. 4, pp. 199-206, 1983.
- [38] M.-H. Bao and Y. Wang, "Analysis and design of a four-terminal silicon pressure sensors at the centre of a diaphragm," *Sensors and Actuators*, vol. 12, pp. 49-56, 1987.
- [39] C. C. Chang, C. T. Lieu, and M. K. Hsieh, "Study of the fabrication of a silicon pressure sensor," *International Journal of Electronics*, vol. 82, pp. 295-302, 1997.
- [40] M. Uematsu, "Simulation of boron, phosphorus, and arsenic diffusion in silicon based on an integrated diffusion model, and the anomalous phosphorus diffusion mechanism," *Journal of Applied Physics*, vol. 82, pp. 2228-2246, 1997.
- [41] M. J. Madou, "MEMS Fabrication," in *The MEMS Handbook*, vol. 16, M. Gad-el-Hak, Ed. Boca Raton: CRC Press, 2002, pp. 1-183.